

Benchmarking Graph Neural Networks

Vijay Prakash Dwivedi^{1*}
vijaypra001@e.ntu.edu.sg

Chaitanya K. Joshi^{1*}
chaitanya.joshi@ntu.edu.sg

Thomas Laurent²
tlaurent@lmu.edu

Yoshua Bengio^{3,4}
yoshua.bengio@mila.quebec

Xavier Bresson¹
xbresson@ntu.edu.sg

¹ School of Computer Science and Engineering, Nanyang Technological University, Singapore

² Department of Mathematics, Loyola Marymount University

³ Mila, University of Montréal ⁴ CIFAR

Abstract

Graph neural networks (GNNs) have become the standard toolkit for analyzing and learning from data on graphs. As the field grows, it becomes critical to identify key architectures and validate new ideas that generalize to larger, more complex datasets. Unfortunately, it has been increasingly difficult to gauge the effectiveness of new models in the absence of a standardized benchmark with consistent experimental settings. In this paper, we introduce a reproducible GNN benchmarking framework², with the facility for researchers to add new models conveniently for arbitrary datasets. We demonstrate the usefulness of our framework by presenting a principled investigation into the recent Weisfeiler-Lehman GNNs (WL-GNNs) compared to message passing-based graph convolutional networks (GCNs) for a variety of graph tasks, i.e. graph regression/classification and node/link prediction, with medium-scale datasets.

1 Introduction

In the last few years, graph neural networks (GNNs) have seen a great surge of interest with promising methods being developed for myriad of domains including chemistry [25, 31], physics [20, 73], social sciences [44, 65], knowledge graphs [76, 16], recommendation [64, 91], and neuroscience [32]. Historically, three classes of GNNs have been developed. The first models [75, 14, 22, 78, 44, 33] aimed at extending the original convolutional neural networks [49, 50] to graphs. The second class enhanced the original models with anisotropic operations on graphs [69], such as attention and gating mechanisms [8, 57, 63, 80, 11]. The recent third class has introduced GNNs that improve upon theoretical limitations of previous models [89, 66, 58, 18, 67, 77]. Specifically, the first two classes can only differentiate simple non-isomorphic graphs and cannot separate automorphic nodes. Developing powerful and theoretically expressive GNN architectures is a key concern towards practical applications and real-world adoption of graph machine learning. However, tracking recent progress has been challenging as most models are evaluated on small datasets such as Cora, Citeseer and TU, which are inappropriate to differentiate complex, simple and graph-agnostic architectures [35, 17], and do not have consensus on a unifying experimental setting [26, 87].

Consequently, our motivation is to benchmark GNNs to identify and quantify what types of architectures, first principles or mechanisms are universal, generalizable, and scalable when we move to larger and more challenging datasets. Benchmarking provides a strong paradigm to answer these

*Equal contribution

²<https://github.com/graphdeeplearning/benchmarking-gnns>

fundamental questions. It has proved to be beneficial for driving progress, identifying essential ideas, and solving domain-specific problems in several areas of science [86]. Recently, the famous 2012 ImageNet challenge [24] has provided a benchmark dataset that has triggered the deep learning revolution [48, 55]. Nevertheless, designing successful benchmarks is highly challenging as it requires both a coding framework with a rigorous experimental setting for fair comparisons, all while being reproducible, as well as using appropriate datasets that can statistically separate model performance. The lack of benchmarks has been a major issue in GNN literature as the aforementioned requirements have not been rigorously enforced.

A major contribution of this work is to design a benchmark infrastructure that can fairly evaluate GNN architectures on medium-scale datasets. Specifically, the coding infrastructure can be used to implement new GNNs from the most popular and theoretically designed classes of GNNs, and compare their performance in a rigorous manner. For nomenclature, we refer to the popular message-passing GNNs as graph convolutional networks (GCNs) and the theoretically expressive GNNs as Weisfeiler-Lehman GNNs (WL-GNNs), see Section 2.2. The main findings of our extensive numerical experiments are presented in Section 4, and summarized below:

- Message-passing GCNs [44, 33, 63, 80, 11] are able to better leverage the basic building blocks of deep learning such as batching, residual connections and normalization, outperforming theoretically designed WL-GNNs [89, 58, 18] on the 7 datasets considered in this paper.
- Theoretically designed WL-GNNs such as [58, 18] are prohibitive in terms of time/space complexity and not amenable to batched training, suggesting the need for additional developments for these models to be competitive with GCNs on practical tasks. In contrast, GCNs rely on sparse matrix computations, which are computationally and memory efficient.
- Overall, anisotropic GCNs which leverage attention [80] and gating [11] mechanisms perform consistently across graph, node and edge-level tasks, improving over isotropic GCNs on 5 out of 7 datasets. Additionally, for link prediction tasks, learning features for edges as joint representations of incident nodes during message passing significantly boosts performance. Their consistent results suggest further analysis on the expressivity of anisotropic models.
- Graph positional encodings with Laplacian eigenvectors [9] are an elegant approach to overcome the theoretical limitation of low structural expressivity of GCNs [67, 77], and boost performance on 3 out of 4 datasets without positional information.

Our benchmarking framework and medium-scale datasets are open-sourced via GitHub to enable researchers to seamlessly explore new ideas in graph representation learning and track the progress of GNN architectures.

2 Proposed GNN Benchmarking Framework

2.1 Coding Infrastructure

Designing successful benchmarks requires a modular coding framework which is experimentally rigorous and reproducible for fair comparisons. However, recent literature on GNNs does not have a consensus on training, validation and test splits as well as evaluation protocols, making it unfair to compare the performance of new ideas and architectures [26]. Additionally, different hyperparameters, loss functions and learning rate schedules make it difficult to identify new advances in architectures. It is also unclear how to perform good data splits on graphs beyond randomizes splits, which are known to provide over-optimistic predictions [53]. A unifying experimental setting is much needed given the heterogeneity in GNN evaluation procedures.

Our benchmarking infrastructure builds upon PyTorch [68] and DGL [85], and has been developed with the following fundamental objectives: (a) Ease-of-use and modularity, enabling new users to experiment and study the building blocks of GNNs; (b) Experimental rigour and fairness for all models being benchmarked; and (c) Being future-proof and comprehensive for tracking the progress of graph machine learning tasks and new GNNs. At a high level, our benchmark unifies independent components for: (i) Data pipelines; (ii) GNN layers and models; (iii) Training and evaluation functions; (iv) Network and hyperparameter configurations; and (v) Scripts for reproducibility. We believe that a standardized framework can be of immense help to the community, enabling researchers to explore new ideas at any stage of the pipeline without setting up everything else. We direct readers

to the README user manual included in our GitHub repository for detailed instructions on using the coding infrastructure.

2.2 Graph Neural Networks

We benchmark two broad classes of GNNs. Firstly, we consider the widely used message passing-based graph convolutional networks (GCNs), which update node representations from one layer to the other according to the formula: $h_i^{\ell+1} = f(h_i^\ell, \{h_j^\ell\}_{j \in \mathcal{N}_i})$. Note that the update equation is *local*, only depending on the neighborhood \mathcal{N}_i of node i , and *independent of graph size*, making the space/time complexity $O(E)$ reducing to $O(n)$ for sparse graphs. Thus, GCNs are highly parallelizable on GPUs and are implemented via sparse matrix multiplications in modern graph machine learning frameworks [85, 27]. GCNs draw parallels to ConvNets for computer vision [50] by considering a convolution operation with shared weights across the graph domain. We instantiate a class of *isotropic* GCNs when the node update equation treats every “edge direction” equally, *i.e.* each neighbor contributes equally to the update of the central node by receiving the same weight value:

$$h_i^{\ell+1} = \sigma\left(W_1^\ell h_i^\ell + \sum_{j \in \mathcal{N}_i} W_2^\ell h_j^\ell\right), \quad h^\ell, h^{\ell+1} \in \mathbb{R}^{n \times d}, \quad W_{1,2}^\ell \in \mathbb{R}^{d \times d}, \quad (1)$$

where σ is a non-linear point-wise activation like ReLU. Popular isotropic GCNs include vanilla GCNs—Graph Convolutional Networks [78, 44] and GraphSage [33]. On the other hand, when the update equation treats every edge direction differently, we instantiate *anisotropic* GCNs:

$$h_i^{\ell+1} = \sigma\left(W_1^\ell h_i^\ell + \sum_{j \in \mathcal{N}_i} \eta_{ij} W_2^\ell h_j^\ell\right), \quad h^\ell, h^{\ell+1} \in \mathbb{R}^{n \times d}, \quad W_{1,2}^\ell \in \mathbb{R}^{d \times d}, \quad (2)$$

where $\eta_{ij} = f^\ell(h_i^\ell, h_j^\ell)$ and f^ℓ is a parameterized function whose weights are learned during training. The η_{ij} can be scalars or vectors. In the latter case the multiplication between the term η_{ij} and the term $W_2^\ell h_j^\ell$ should be understood as element-wise multiplication. MoNet—Gaussian Mixture Model Networks [63], GatedGCN—Graph Convolutional Networks [11], and GAT—Graph Attention Networks [80] propose edge weights based on GMMs, gating mechanism and sparse attention for computing η_{ij} , respectively.

The second class we investigate is the recent *Weisfeiler-Lehman* GNNs based on the WL test [88]. Authors in [89] introduced GIN—Graph Isomorphism Network, a provable 1-WL GNN, which can distinguish two non-isomorphic graphs w.r.t. the 1-WL test. Higher k -WL isomorphic tests lead to more discriminative k -WL GNNs in [66, 58]. However, k -WL GNNs require the use of tensors of rank k , which is intractable in practice for $k > 2$. As a result, [58] proposed a model, namely 3-WL GNNs, that uses rank-2 tensors while being 3-WL provable. This 3-WL model improves the space/time complexities of [66] from $O(n^3)/O(n^4)$ to $O(n^2)/O(n^3)$ respectively. The layer update equation of 3-WL GNNs is defined as:

$$h^{\ell+1} = \text{Concat}\left(M_{W_1^\ell}(h^\ell), M_{W_2^\ell}(h^\ell), M_{W_3^\ell}(h^\ell)\right), \quad h^\ell, h^{\ell+1} \in \mathbb{R}^{n \times n \times d}, \quad W_{1,2,3}^\ell \in \mathbb{R}^{d \times d \times 2}, \quad (3)$$

where M_W are 2-layer MLPs applied to the feature dimension. Authors in [18] proposed RingGNNs, which also use rank-2 tensors and achieve higher learning capacity than 2-WL GNNs. The layer update equation of RingGNN is:

$$h^{\ell+1} = \sigma\left(w_1^\ell L_{W_1^\ell}(h^\ell) + w_2^\ell L_{W_2^\ell}(h^\ell) \cdot L_{W_3^\ell}(h^\ell)\right), \quad h^\ell, h^{\ell+1} \in \mathbb{R}^{n \times n \times d}, \quad W_{1,2,3}^\ell \in \mathbb{R}^{d \times d \times 17}, \quad (4)$$

and $w_{1,2}^\ell \in \mathbb{R}$. This model uses the equivariant linear layer L_W defined in [59] as $L_W(h)_{\cdot, \cdot, k} = \sum_{i=1}^{17} \sum_{j=1}^d W_{i,j,k} L_i(h)_{\cdot, \cdot, j}$, where $\{L_i\}_{i=1}^{15}$ is the set of all basis functions for all linear equivariant functions from $\mathbb{R}^{n \times n} \rightarrow \mathbb{R}^{n \times n}$ and $\{L_i\}_{i=16}^{17}$ are the basis for the bias terms. RingGNNs have the same space/time complexities as 3-WL GNNs. We refer the readers to the supplementary material for detailed formulations of these models.

All GCNs can be upgraded with basic building blocks of deep networks, *i.e.* residual connections [34, 51] and batch normalization [36]. We discuss batch normalization and residual connections for WL-GNNs in Section 4.

Table 1: Summary statistics of datasets included in the proposed benchmark.

Domain & Construction	Dataset	#Graphs	#Nodes	Total #Nodes	Task
Chemistry: Real-world molecular graphs	ZINC	12K	9-37	277,864	Graph Regression
Mathematical Modelling: Artificial graphs generated from Stochastic Block Models	PATTERN CLUSTER	14K 12K	44-188 41-190	1,664,491 1,406,436	Node Classification
Computer Vision: Graphs constructed with SLIC super-pixels of images	MNIST CIFAR10	70K 60K	40-75 85-150	4,939,668 7,058,005	Graph Classification
Combinatorial Optimization: Uniformly generated artificial Euclidean graphs	TSP	12K	50-500	3,309,140	Edge Classification
Social Networks: Real-world citation graph	COLLAB	1	235,868	235,868	Edge Classification
Circular Skip Links: Isomorphic graphs with same degree	CSL	150	41	6,150	Graph Classification

2.3 Datasets

Issues with Prevalent Datasets. New ideas in the field of GNNs have mostly been evaluated on the realistic but small scale Cora [61], Citeseer [30] and TU datasets [41]. For example, Cora is a single graph of 2.7K nodes, TU-IMDB has 1.5K graphs with 13 nodes on average and TU-MUTAG has 188 molecules with 18 nodes. Although small datasets are useful as sanity checks for new ideas, they can become a liability in the long run as new GNN models will be designed to overfit the small test sets instead of searching for more generalizable architectures. As mentioned previously, another major issue with prevalent datasets is the lack of reproducibility of experimental results. Most published papers do not use the same train-validation-test split [26]. Besides, even for the same split, the performance of GNNs present a large standard deviation on a regular 10-fold cross-validation due to the small size, see supplementary material.

At the same time, collecting representative, realistic and large scale graph datasets presents several challenges. It is unclear what theoretical tools can define the quality of a dataset or validate its statistical representativeness for a given task. Additionally, there are several arbitrary choices when preparing graphs, such as node and edge features. For example, e-commerce product features can be given by a specialized bag-of-words, or computed from word embeddings from the title as well as description. Finally, it is unclear how to classify dataset size/scale as the appropriate size may depend on the complexity of the task as well as the dimensionality and statistics of underlying data. Very large graph datasets also present a computational challenge and require extensive GPU resources to be studied [19, 71]. The recent Open Graph Benchmark (OGB) project [87] is a much needed initiative in the community to tackle these challenges. OGB offers a collection of medium-scale real-world graph machine learning datasets and evaluation protocols, with an emphasis on out-of-distribution generalization performance through meaningful data splits.

Proposed Datasets. In our benchmark, we define *appropriate datasets* as those that are able to statistically separate the performance of GNNs. It is important to note that small datasets like Cora, Citeseer and TU datasets do not fulfil this requirement, as all GNNs perform almost statistically the same. Table 1 presents a summary of 7 medium-scale datasets and one small-scale dataset included in our benchmarking framework. We cover the four most fundamental supervised graph machine learning tasks [15]: graph regression (ZINC), graph classification (MNIST, CIFAR10, CSL), node classification (PATTERN, CLUSTER), and link prediction (TSP, COLLAB), coming from the domains of chemistry, mathematical modelling, computer vision, combinatorial optimization, and social networks. Four datasets (PATTERN, CLUSTER, TSP, CSL) are artificially generated, two datasets (MNIST, CIFAR10) are semi-artificial, and two (ZINC, COLLAB) are real-world datasets. The dataset sizes in terms of total number of nodes vary between 0.27M to 7M.

Relevance. ZINC [37] is one of the most popular real-world molecular dataset of 250K graphs, out of which we randomly select 12K for efficiency. We consider the task of graph property regression for constrained solubility, an important chemical property for designing generative GNNs for molecules [39, 92]. PATTERN and CLUSTER are node classification tasks generated with Stochastic Block Models [1], which are widely used to model communities in social networks by modulating the intra- and extra-communities connections, thereby controlling the difficulty of the task. PATTERN tests the fundamental graph task of recognizing specific predetermined subgraphs (as proposed in [75]) and CLUSTER aims at identifying community clusters in a semi-supervised setting [44]. All SBM graphs are augmented with node features to simulate user attributes such that

the tasks are more natural and not purely structural clustering tasks. **MNIST** [50] and **CIFAR10** [47] are classical image classification datasets converted into graphs using so called super-pixels [2] and assigning each node’s features as the super-pixel coordinates and intensity. These datasets are sanity-checks, as we expect most GNNs to perform close to 100% for MNIST and well enough for CIFAR10. **TSP**, based on the classical *Travelling Salesman Problem*, tests link prediction on 2D Euclidean graphs to identify edges belonging to the optimal TSP solution given by the Concorde solver [4]. TSP is the most intensely studied NP-Hard combinatorial problem with a growing body of literature on leveraging GNNs to learn better solvers [42, 40, 10]. **COLLAB** is a link prediction dataset proposed by OGB [87] corresponding to a collaboration network between scientists indexed by Microsoft Academic Graph [84]. The task is to predict future author collaboration relationships given past collaboration links. Lastly, **CSL** is a synthetic dataset introduced in [67] to test the expressivity of GNNs. In particular, graphs are isomorphic if they have the same degree and the task is to classify non-isomorphic graphs.

Finally, it is worth noting that our benchmarking infrastructure is complementary to the OGB initiative, and is well-suited to integrate current and future OGB dataset and evaluation protocols, as demonstrated by the inclusion of the COLLAB dataset.

3 Experimental Setting

Data splitting. ZINC has 10K train/1K validation/1K and 1K test graphs. For MNIST and CIFAR10, the statistics are respectively 55K train/5K validation/10K test, and 45K train/5K validation/10K test. The 5K samples for the validation set in both MNIST and CIFAR10 are sampled randomly from the respective train sets. The numbers of SBM graphs are 10K train/2K validation/2K test for PATTERN and 10K train/1K validation/1K test for CLUSTER. Similarly, TSP has 10K train/1K validation and 1K test graphs. COLLAB is a single large temporal graph of size 235K nodes with train/validation/test edge splits provided by OGB. Finally, CSL has 150 graphs and we follow 5-fold cross validation with stratified sampling to ensure class distribution remains the same across the splits. See supplementary for more details on generation and preparation of the datasets.

Training. We use the Adam optimizer [43] with the same learning rate decay strategy for all models. An initial learning rate is selected in $\{10^{-3}, 10^{-4}\}$ which is reduced by half if the validation loss does not improve after a fixed number of epochs, either 5 or 10. We do not set a maximum number of epochs – the training is stopped either when the learning rate has reached the small value of 10^{-6} , or the computational time reaches 12 hours. We run each experiment with 4 different seeds and report the statistics of the 4 results. More details are provided in the supplementary.

Task-based network layer. The node representations generated by the final layer of GCNs, or the dense tensor obtained at the final layer of the higher order WL-GNNs, are passed to a network suffix which is usually a downstream MLP of 3 layers. For GIN, RingGNN, and 3WL-GNN, we follow the original instructions of network suffixes to consider feature outputs from each layer of the network, similar to that of Jumping Knowledge Networks [90]. See supplementary material for more details.

Parameter budgets. Our goal is not to find the optimal set of hyperparameters for a specific GNN model (which is computationally expensive), but to compare and benchmark the model and/or their building blocks within a budget of parameters and a maximal computational time. Therefore, we decide on using two parameter budgets: (1) 100k parameters for each GNNs for all the tasks, and (2) 500k parameters for GNNs for which we investigate scaling a model to larger parameters and deeper layers. The number of hidden layers and hidden dimensions are selected accordingly to match these budgets, the details of which are in the supplementary material.

4 Benchmarking GNNs

This section highlights the main take-home messages from the experiments in Tables 2, 3 and 4, which evaluate the GNNs from Section 2.2 with the experimental setup described in Section 3.

Graph-agnostic NNs perform poorly. As a sanity check, we compare all GNNs to a simple graph-agnostic MLP baseline which updates each node independent of one-other, $h_i^{\ell+1} = \sigma(W^\ell h_i^\ell)$, and passes these features to the task-based layer. MLP presents consistently low scores across all datasets (Tables 2 and 3), which shows the necessity to use graph structure for these tasks. All proposed

Table 2: Benchmarking results for MP-GCNs and WL-GNNs across 7 medium-scale graph classification/regression and node/link prediction datasets. Results are averaged over 4 runs with 4 different seeds. **Red**: the best model, **Violet**: good models.

NODE CLASSIFICATION											
Model	L	#Param	Test Acc. \pm s.d.	PATTERN Train Acc. \pm s.d.	#Epoch	Epoch/Total	#Param	Test Acc. \pm s.d.	CLUSTER Train Acc. \pm s.d.	#Epoch	Epoch/Total
MLP	4	105263	50.519 \pm 0.000	50.487 \pm 0.014	42.25	8.95s/0.11hr	106015	20.973 \pm 0.004	20.938 \pm 0.002	42.25	5.83s/0.07hr
GCN	4	100923	63.880 \pm 0.074	65.126 \pm 0.135	105.00	118.85s/3.51hr	101655	53.445 \pm 2.029	54.041 \pm 2.197	70.00	65.72s/1.30hr
GraphSage	16	500823	71.892 \pm 0.334	78.409 \pm 1.592	81.50	492.19s/11.31hr	501687	68.498 \pm 0.976	71.729 \pm 2.212	79.75	270.28s/6.08hr
	4	101739	50.516 \pm 0.001	50.473 \pm 0.014	43.75	93.41s/1.17hr	102187	50.454 \pm 0.145	54.374 \pm 0.203	64.00	53.56s/0.97hr
	16	502842	50.492 \pm 0.001	50.487 \pm 0.005	46.50	391.19s/5.19hr	503350	63.844 \pm 0.110	86.710 \pm 0.167	57.75	225.61s/3.70hr
MoNet	4	103775	85.482 \pm 0.037	85.569 \pm 0.044	89.75	35.71s/0.90hr	104227	58.064 \pm 0.131	58.454 \pm 0.183	76.25	24.29s/0.52hr
GAT	16	511487	85.582 \pm 0.038	85.720 \pm 0.068	81.75	68.49s/1.58hr	511999	66.407 \pm 0.540	67.727 \pm 0.649	77.75	47.82s/1.05hr
	4	109936	75.824 \pm 1.823	77.883 \pm 1.632	96.00	20.92s/0.57hr	110700	57.732 \pm 0.323	58.331 \pm 0.342	67.25	14.17s/0.27hr
	16	526990	78.271 \pm 0.186	90.212 \pm 0.476	53.50	50.33s/0.77hr	527874	70.587 \pm 0.447	76.074 \pm 1.362	73.50	35.94s/0.75hr
GatedGCN	4	104003	84.480 \pm 0.122	84.474 \pm 0.155	78.75	139.01s/3.09hr	104355	60.404 \pm 0.419	61.618 \pm 0.536	94.50	79.97s/1.81hr
GatedGCN-PE	16	502223	85.568 \pm 0.088	86.007 \pm 0.123	65.25	644.71s/11.91hr	502615	73.840 \pm 0.326	87.880 \pm 0.908	60.00	400.07s/6.13hr
	4	502457	86.508 \pm 0.085	86.801 \pm 0.133	65.75	647.94s/12.08hr	504253	76.082 \pm 0.196	88.919 \pm 0.720	57.75	399.66s/6.58hr
GIN	4	100884	85.590 \pm 0.011	85.852 \pm 0.030	93.00	15.24s/0.40hr	103544	58.384 \pm 0.236	59.480 \pm 0.337	74.75	10.71s/0.22hr
RingGNN	16	508574	85.387 \pm 0.136	85.664 \pm 0.116	86.75	25.14s/0.62hr	517570	64.716 \pm 1.553	65.973 \pm 1.816	80.75	20.67s/0.47hr
	2	105206	86.245 \pm 0.013	86.118 \pm 0.034	75.00	573.37s/12.17hr	104746	42.418 \pm 20.063	42.520 \pm 20.212	74.50	428.24s/8.79hr
3WLGNN	2	504766	86.244 \pm 0.025	86.105 \pm 0.021	72.00	595.97s/12.15hr	524202	22.340 \pm 0.000	22.304 \pm 0.000	43.25	501.84s/6.22hr
	8	505749	Diverged	Diverged	Diverged	Diverged	514380	Diverged	Diverged	Diverged	Diverged
3WLGNN	3	103572	85.661 \pm 0.353	85.608 \pm 0.337	95.00	304.79s/7.88hr	105552	57.130 \pm 6.539	57.404 \pm 6.597	116.00	219.51s/6.52hr
	3	502872	85.341 \pm 0.207	85.270 \pm 0.198	81.75	424.23s/9.56hr	507252	55.489 \pm 7.863	55.736 \pm 8.024	66.00	319.98s/5.79hr
	8	581716	Diverged	Diverged	Diverged	Diverged	586788	Diverged	Diverged	Diverged	Diverged

GRAPH CLASSIFICATION											
Model	L	#Param	Test Acc. \pm s.d.	MNIST Train Acc. \pm s.d.	#Epoch	Epoch/Total	#Param	Test Acc. \pm s.d.	CIFAR10 Train Acc. \pm s.d.	#Epoch	Epoch/Total
MLP	4	104044	95.340 \pm 0.138	97.432 \pm 0.470	232.25	22.74s/1.48hr	104380	56.340 \pm 0.181	65.113 \pm 1.685	185.25	29.48s/1.53hr
GCN	4	101365	90.705 \pm 0.218	97.196 \pm 0.223	127.50	83.41s/2.99hr	101657	55.710 \pm 0.381	69.523 \pm 1.948	142.50	109.63s/4.39hr
GraphSage	4	104337	97.312 \pm 0.097	100.000 \pm 0.000	98.25	113.12s/3.13hr	104517	65.767 \pm 0.308	99.719 \pm 0.062	93.50	124.61s/2.93hr
MoNet	4	104049	90.805 \pm 0.032	96.609 \pm 0.440	146.25	93.19s/3.82hr	104229	54.655 \pm 0.518	65.911 \pm 2.515	141.50	97.13s/3.85hr
GAT	4	110400	95.535 \pm 0.205	99.994 \pm 0.008	104.75	42.26s/1.25hr	110704	64.223 \pm 0.455	89.114 \pm 0.499	103.75	55.27s/1.62hr
GatedGCN	4	104217	97.340 \pm 0.143	100.000 \pm 0.000	96.25	128.79s/3.50hr	104357	67.312 \pm 0.311	94.553 \pm 1.018	97.00	154.15s/4.22hr
GIN	4	105434	96.485 \pm 0.252	100.000 \pm 0.000	128.00	39.22s/1.41hr	105654	55.255 \pm 1.527	79.412 \pm 9.700	141.50	52.12s/0.77hr
RingGNN	2	105398	11.350 \pm 0.000	11.235 \pm 0.000	14.00	2945.69s/12.77hr	105165	19.300 \pm 16.108	19.556 \pm 16.397	13.50	3112.96s/13.00hr
	2	505182	91.860 \pm 0.449	92.169 \pm 0.505	16.25	2575.99s/12.63hr	504949	39.165 \pm 17.114	40.209 \pm 17.790	13.75	2998.24s/12.06hr
3WLGNN	8	506357	Diverged	Diverged	Diverged	Diverged	510439	Diverged	Diverged	Diverged	Diverged
	3	108024	95.075 \pm 0.961	95.830 \pm 1.338	27.75	1523.20s/12.40hr	108516	59.175 \pm 1.593	63.751 \pm 2.697	28.50	1506.29s/12.60hr
3	501690	95.002 \pm 0.419	95.692 \pm 0.677	26.25	1608.73s/12.42hr	502770	58.043 \pm 2.512	61.574 \pm 3.575	20.00	2091.22s/12.55hr	
8	500816	Diverged	Diverged	Diverged	Diverged	Diverged	501584	Diverged	Diverged	Diverged	Diverged

LINK PREDICTION											
Model	L	#Param	Test F1 \pm s.d.	TSP Train F1 \pm s.d.	#Epoch	Epoch/Total	#Param (L = 3)	Test Hits \pm s.d.	COLLAB Train Hits \pm s.d.	#Epoch	Epoch/Total
MLP	4	96956	0.544 \pm 0.001	0.544 \pm 0.001	164.25	50.15s/2.31hr	39441	20.350 \pm 2.168	29.807 \pm 3.360	147.50	2.09s/0.09hr
GCN	4	95702	0.630 \pm 0.001	0.631 \pm 0.001	261.00	152.89s/11.15hr	40479	50.422 \pm 1.131	92.112 \pm 0.991	122.50	351.05s/12.04hr
GraphSage	4	99263	0.665 \pm 0.003	0.669 \pm 0.003	266.00	157.26s/11.68hr	39856	51.618 \pm 0.690	99.949 \pm 0.052	152.75	279.93s/11.87hr
MoNet	4	99007	0.641 \pm 0.002	0.643 \pm 0.002	282.00	84.46s/6.65hr	39751	36.144 \pm 2.191	61.156 \pm 3.973	167.50	26.69s/1.26hr
GAT	4	96182	0.671 \pm 0.002	0.673 \pm 0.002	328.25	68.23s/6.25hr	42637	51.501 \pm 0.962	97.851 \pm 1.114	157.00	18.12s/0.80hr
GatedGCN	4	97858	0.791 \pm 0.003	0.793 \pm 0.003	159.00	218.20s/9.72hr	40965	52.635 \pm 1.168	96.103 \pm 1.876	95.00	453.47s/12.09hr
GatedGCN-PE	4	97858	0.808 \pm 0.003	0.811 \pm 0.003	197.00	218.51s/12.04hr	41889	52.849 \pm 1.345	96.165 \pm 0.453	94.75	452.75s/12.08hr
GatedGCN-E	16	500770	0.838 \pm 0.002	0.850 \pm 0.001	53.00	807.23s/12.17hr	40965	49.212 \pm 1.560	88.747 \pm 1.058	95.00	451.21s/12.03hr
GIN	4	99002	0.656 \pm 0.003	0.660 \pm 0.003	273.50	72.73s/5.56hr	39544	41.730 \pm 2.284	70.555 \pm 4.444	140.25	8.66s/0.34hr
RingGNN	2	106862	0.643 \pm 0.024	0.644 \pm 0.024	2.00	17850.52s/17.19hr	-	OOM	-	-	-
	2	507938	0.704 \pm 0.003	0.705 \pm 0.003	3.00	12835.53s/16.08hr	-	OOM	-	-	-
3WLGNN	8	506564	Diverged	Diverged	Diverged	Diverged	-	OOM	-	-	-
	3	106366	0.694 \pm 0.073	0.695 \pm 0.073	2.00	17468.81s/16.59hr	-	OOM	-	-	-
	3	506681	0.288 \pm 0.311	0.290 \pm 0.312	2.00	17190.17s/16.51hr	-	OOM	-	-	-
	8	508832	OOM	OOM	OOM	OOM	-	OOM	-	-	-

k-NN Heuristic		k = 2	Test F1: 0.693	-			60546561	44.206 \pm 0.452	100.000 \pm 0.000	254.33	2.66s/0.21hr
Matrix Fact.	0	-	-	-	-	-	-	-	-	-	-

GRAPH REGRESSION - ZINC											
Model	L	#Param	Test MAE \pm s.d.	Train MAE \pm s.d.	#Epoch	Epoch/Total					
MLP	4	108975	0.706 \pm 0.006	0.644 \pm 0.005	116.75	1.01s/0.03hr					
GCN	4	103077	0.459 \pm 0.006	0.343 \pm 0.011	196.25	2.89s/0.16hr					
GraphSage	16	505079	0.367 \pm 0.011	0.128 \pm 0.019	197.00	12.78s/0.71hr					
	4	94977	0.468 \pm 0.003	0.251 \pm 0.004	147.25	3.74s/0.15hr					
MoNet	16	505341	0.398 \pm 0.002	0.081 \pm 0.009	145.50	16.61s/0.68hr					
	4	106002	0.397 \pm 0.010	0.318 \pm 0.016	188.25	1.97s/0.10hr					
GAT	16	504013	0.292 \pm 0.006	0.093 \pm 0.014	171.75	10.82s/0.52hr					
	4	102385	0.475 \pm 0.007	0.317 \pm 0.006	137.50	2.93s/0.11hr					
GatedGCN	16	531345	0.384 \pm 0.007	0.067 \pm 0.004	144.00	12.98s/0.53hr					
	4	105735	0.435 \pm 0.011	0.287 \pm 0.014	173.50	5.76s/0.28hr					
GatedGCN-E	4	105875	0.375 \pm 0.003	0.236 \pm 0.007	194.75	5.37s/0.29hr					
GatedGCN-E-PE	16	504309	0.282 \pm 0.015	0.074 \pm 0.016	166.75	20.50s/0.96hr					
	16	505011	0.214 \pm 0.013	0.067 \pm 0.019	185.00	10.70s/0.56hr					
GIN	4	103079	0.387 \pm 0.015	0.319 \pm 0.015	153.25	2.29s/0.10hr					
RingGNN	16	509549	0.526 \pm 0.051	0.444 \pm 0.039	147.00	10.22s/0.42hr					
	2	97978	0.512 \pm 0.023	0.383 \pm 0.020	90.25	327.65s/8.32hr					
RingGNN-E	2	104403	0.363 \pm 0.026	0.243 \pm 0.025	95.00	366.29s/9.76hr					
	2	527283	0.353 \pm 0.019	0.236 \pm 0.019	79.75	293.94s/6.63hr					
3WLGNN	8	510305	Diverged	Diverged	Diverged	Diverged					
	3	102150	0.407 \pm 0.028	0.272 \pm 0.037	111.25	286.23s/8.88hr					
3WLGNN-E	3	103098	0.256 \pm 0.054	0.140 \pm 0.044	117.25	334.69s/10.90hr					
	3	507603	0.303 \pm 0.068	0.173 \pm 0.041	120.25	329.49s/11.08hr					
	8	582824	0.303 \pm 0.057	0.246 \pm 0.043	52.50	81.27s/12.15hr					

Evaluation Metrics: (higher is better, except for ZINC)

- CLUSTER, PATTERN use weighted accuracy w.r.t. the class sizes.
- MNIST, CIFAR10 use multi-label classification accuracy.
- TSP uses binary F1 score for the positive edges.
- COLLAB uses Hits@50 via the evaluator provided by OGB [87].
- ZINC uses mean absolute regression error.

Notation:

- Models with the suffix **-E** use input edge features to initialize edge representations (ZINC: bond type, TSP: Euclidean distance, COLLAB: collaboration frequency and year).
- Models with the suffix **-PE** use Laplacian Eigenvectors as node positional encodings, with dimension 8 for ZINC, 2 for PATTERN and 20 for others.
- Results denoted by **Diverged** indicate unstable and divergent runs across all 4 seeds and initial learning rate values $\{10^{-3}, 10^{-4}, 10^{-5}\}$.
- Results denoted by **OOM** indicate runs which throw out of memory errors on our hardware configuration.

Extended training:

- For TSP, RingGNN/3WLGNN with 100K parameters achieved 0.733 \pm 0.020 and 0.649 \pm 0.051 respectively after 48hr of training.

These new models are limited in terms of space/time complexities, with $O(n^2)/O(n^3)$ respectively, not allowing them to scale to larger datasets. On the contrary, GCNs with linear complexity *w.r.t.* the number of nodes for sparse graphs, can scale conveniently to 16 layers and show the best performance on all datasets. 3WL-GNNs and RingGNNs face loss divergence and/or out-of-memory errors when trying to build deeper networks, see Table 2.

Anisotropic mechanisms improve GCNs. Among the models in the GCN class, the best results point towards the anisotropic models, particularly GAT and GatedGCN, which are based on sparse and dense attention mechanisms, respectively. For instance, results for ZINC, PATTERN, CLUSTER, MNIST and CIFAR in Table 2 show that the performance of the 100K-parameter anisotropic GNNs (GAT, MoNet, GatedGCN) are consistently better than the isotropic models (GCN, GraphSage), except for GraphSage-MNIST and MoNet-CIFAR10. Table 4, discussed later, dissects and demonstrates the importance of anisotropy for the link prediction tasks, TSP and COLLAB. Overall, our results suggest that understanding the expressive power of attention-based neighborhood aggregation functions is a meaningful avenue of research.

Underlying challenges for training WL-GNNs. We consistently observe a relatively high standard deviation in the performance of WL-GNNs (recall that we average across 4 runs using 4 different seeds). We attribute this fluctuation to the absence of universal training procedures like batching and batch normalization, as these GNNs operate on *dense* rank-2 tensors of variable sizes. On the other hand, GCNs running on *sparse* tensors better leverage batched training and normalization for stable and fast training. Leading graph machine learning libraries represent batches of graphs as sparse block diagonal matrices, enabling batched training of GCNs through parallelized computation [38]. Dense tensors are incompatible with the prevalent approach, disabling the use of batch normalization for WL-GNNs. We experimented with layer normalization [5] but without success. We were also unable to train WL-GNNs on CPU memory for the single COLLAB graph. Practical applications of the new WL-GNNs may require redesigning the best practices and common building blocks of deep learning, *i.e.* batching of variable-sized data, normalization schemes, and residual connections.

3WL-GNNs perform the best among their class. Among the models in the WL-GNN class, 3WL-GNN provide better results than its similar counter-part RingGNN. The GIN model, while being less expressive, is able to scale better and provides overall good performance.

Laplacian eigenvectors as positional embeddings. *Background.* In [67, 77], it was pointed out that standard GCNs might perform poorly when dealing with graphs that exhibit some symmetries in their structures, such as node or edge isomorphism. To address this issue, authors in [67] introduced a framework, called Graph Relational Pooling (GRP), that assigns to each node an identifier that depends on the index ordering. This approach can be computationally expensive as it requires to account for all $n!$ node permutations, thus requiring some sampling in practice.

Proposition. As in [67], we keep the overall GCN architecture and simply add positional features to each node before processing the graph through the GCN. The positional features should be chosen such that nodes which are far apart in the graph have different positional features whereas nodes which are nearby have similar positional features. In [67], authors used one-hot encoding of node indices. As an alternative, we propose to use the graph Laplacian eigenvectors [9], which have less ambiguities and which better describe the distance between nodes on the graph. Formally, Laplacian eigenvectors are spectral techniques that embed the graphs into the Euclidean space. These vectors form a meaningful local coordinate system, while preserving the global graph structure. Mathematically, they are defined via the factorization of the graph Laplacian matrix;

$$\Delta = \mathbf{I} - D^{-1/2} A D^{-1/2} = U^T \Lambda U, \quad (5)$$

where A is the $n \times n$ adjacency matrix, D is the degree matrix, and Λ, U correspond respectively to the eigenvalues and eigenvectors. Laplacian eigenvectors also represent a natural generalization of the Transformer [79] positional encodings (PE) for graphs as the eigenvectors of a discrete line (NLP graph) are the cosine and sinusoidal functions. The computational complexity $O(E^{3/2})$, with E being the number of edges, can be improved with, *e.g.* the Nystrom method [28]. The eigenvectors are defined up to the factor ± 1 (after being normalized to unit length), so the sign of eigenvectors will be randomly flipped during training. For the experiments, we use the k smallest non-trivial eigenvectors, where the k value is given in Table 2. The smallest eigenvectors provide smooth encoding coordinates of neighboring nodes. See Section D in the supplementary for a discussion about positional encodings.

Table 3: Results for the CSL dataset, with and without Laplacian Positional Encodings. Results are from 5-fold cross validation, run 20 times with different seeds. **Red**: the best model, **Violet**: good models.

Model	L	#Param	Test Accuracy			Train Accuracy			#Epoch	Epoch/ Total
			Mean \pm s.d.	Max	Min	Mean \pm s.d.	Max	Min		
Node Positional Encoding with Laplacian Eigenmaps										
MLP	4	101235	22.567 \pm 6.089	46.667	10.000	30.389 \pm 5.712	43.333	10.000	109.39	0.16s/0.03hr
GCN	4	103847	100.000\pm0.000	100.000	100.000	100.000 \pm 0.000	100.000	100.000	125.64	0.40s/0.07hr
GraphSage	4	105867	99.933\pm0.467	100.000	96.667	100.000 \pm 0.000	100.000	100.000	155.00	0.50s/0.11hr
MoNet	4	105579	99.967\pm0.332	100.000	96.667	100.000 \pm 0.000	100.000	100.000	130.39	0.49s/0.09hr
GAT	4	101710	99.933\pm0.467	100.000	96.667	100.000 \pm 0.000	100.000	100.000	133.18	0.61s/0.12hr
GatedGCN	4	105407	99.600\pm1.083	100.000	96.667	100.000 \pm 0.000	100.000	100.000	147.06	0.66s/0.14hr
GIN	4	107304	99.333\pm1.333	100.000	96.667	100.000 \pm 0.000	100.000	100.000	62.98	0.44s/0.04hr
RingGNN	2	102726	17.233 \pm 6.326	40.000	10.000	26.122 \pm 14.382	58.889	10.000	122.75	2.93s/0.50hr
	2	505086	25.167 \pm 7.399	46.667	10.000	54.533 \pm 18.415	82.222	10.000	120.58	3.11s/0.51hr
3WLGNN	3	102054	30.533 \pm 9.863	56.667	10.000	99.644 \pm 1.684	100.000	88.889	74.66	2.33s/0.25hr
	3	505347	30.500 \pm 8.197	56.667	13.333	100.000 \pm 0.000	100.000	100.000	66.64	2.38s/0.23hr
No Node Positional Encoding										
MP-GNNs	4	100K	10.000 \pm 0.000	10.000	10.000	10.000 \pm 0.000	10.000	10.000	-	-
RingGNN	2	101138	10.000 \pm 0.000	10.000	10.000	10.000 \pm 0.000	10.000	10.000	103.23	3.09s/0.45hr
	2	505325	10.000 \pm 0.000	10.000	10.000	10.000 \pm 0.000	10.000	10.000	90.04	3.28s/0.42hr
3WLGNN	3	102510	95.700 \pm 14.850	100.000	30.000	95.700 \pm 14.850	100.000	30.000	475.81	2.29s/1.51hr
	3	506106	97.800 \pm 10.916	100.000	30.000	97.800 \pm 10.916	100.000	30.000	283.80	2.28s/0.90hr

Table 4: Study of anisotropy and edge representations for link prediction on TSP and COLLAB. **Red**: the best model, **Violet**: good models.

	Model	E.Feat.	E.Repr.	L	#Param	Test Acc. \pm s.d.	Train Acc. \pm s.d.	#Epochs	Epoch/Total
TSP	GatedGCN	x	x	4	99026	0.646 \pm 0.002	0.648 \pm 0.002	197.50	150.83s/8.34hr
		✓	x	4	98174	0.757 \pm 0.009	0.760 \pm 0.009	218.25	197.80s/12.06hr
		✓	✓	4	97858	0.791\pm0.003	0.793 \pm 0.003	159.00	218.20s/9.72hr
	GatedGCN-E	✓	✓	4	97858	0.808\pm0.003	0.811 \pm 0.003	197.00	218.51s/12.04hr
		x	x	4	95462	0.643 \pm 0.001	0.644 \pm 0.001	132.75	325.22s/12.10hr
		✓	x	4	96182	0.671 \pm 0.002	0.673 \pm 0.002	328.25	68.23s/6.25hr
		✓	✓	4	96762	0.748 \pm 0.022	0.749 \pm 0.022	93.00	462.22s/12.10hr
	GAT-E	✓	✓	4	96762	0.782\pm0.006	0.783 \pm 0.006	98.00	438.37s/12.11hr
COLLAB	GatedGCN	x	x	3	26593	35.989 \pm 1.549	60.586 \pm 4.251	148.00	263.62s/10.90hr
		✓	x	3	26715	50.668\pm0.291	96.128 \pm 0.576	172.00	384.39s/18.44hr
		✓	✓	3	27055	51.537\pm1.038	96.524 \pm 1.704	188.67	376.67s/19.85hr
	GatedGCN-E	✓	✓	3	27055	47.212 \pm 2.016	85.801 \pm 0.984	156.67	377.04s/16.49hr
		x	x	3	28201	41.141 \pm 0.701	70.344 \pm 1.837	153.50	371.50s/15.97hr
		✓	x	3	28561	50.662\pm0.687	96.085 \pm 0.499	174.50	403.52s/19.69hr
		✓	✓	3	26676	49.674\pm0.105	92.665 \pm 0.719	201.00	349.19s/19.59hr
	GAT-E	✓	✓	3	26676	44.989 \pm 1.395	82.230 \pm 4.941	120.67	328.29s/11.10hr

Analysis. First, we study the usefulness of these PE with CSL, a mathematical dataset introduced in [67] to demonstrate the failure of GCNs to provide meaningful node representations for highly automorphic graphs. Table 3 compares the GCNs using the Laplacian eigenvectors as PE and the WL-GNNs. The GCN models were the most accurate with 99% of mean accuracy, while 3WL-GNN obtained 97% and RingGNN 25% with our experimental setting. Then, we study ZINC, PATTERN, CLUSTER and COLLAB with PE (note that MNIST, CIFAR10 and TSP do not need PE as the nodes in these graphs already have features describing their positions in \mathbb{R}^2). We observe a boost of performance for ZINC and CLUSTER (it was expected as eigenvectors are good indicators of clusters [82]), an improvement for PATTERN, and statistically the same result for COLLAB, see Table 2. As a future work, we plan to compare with the recent technique [93] which uses GNNs to learn simultaneously node structural and positional encodings.

Edge representations improve link prediction. *Context.* The TSP and COLLAB edge classification tasks present an interesting empirical result for GCNs: Isotropic models (GCN, GraphSage) are consistently outperformed by their Anisotropic counterparts which use joint representations of adjacent nodes as edge features during aggregation (GAT, GatedGCN). In Table 4, we systematically study the impact of anisotropy by instantiating three variants of GAT and GatedGCN:

(1) Isotropic aggregation (such as vanilla GCNs [44]) with node updates of the form:

$$h_i^{\ell+1} = \sigma\left(\sum_{j \in \mathcal{N}_i} W^\ell h_j^\ell\right), \quad \text{identified by } (E.Feat, E.Repr=x, x) \text{ in Table 4;} \quad (6)$$

(2) Anisotropy using edge features (such as GAT by default [80]) with node updates as:

$$h_i^{\ell+1} = \sigma\left(\sum_{j \in \mathcal{N}_i} f_{V^\ell}(h_i^\ell, h_j^\ell) \cdot W^\ell h_j^\ell\right), \quad \text{with } (E.Feat, E.Repr=\checkmark, x); \quad (7)$$

and (3) Anisotropy with edge features and explicit edge representations updated at each layer with node/edge updates as (such as in GatedGCN by default [11]):

$$h_i^{\ell+1} = \sigma\left(\sum_{j \in \mathcal{N}_i} e_{ij}^\ell \cdot W^\ell h_j^\ell\right), \quad e_{ij}^{\ell+1} = f_{V^\ell}(h_i^\ell, h_j^\ell, e_{ij}^\ell), \quad \text{with } (E.Feat, E.Repr = \checkmark, \checkmark). \quad (8)$$

GatedGCN-E and GAT-E in Table 4 are models using input edge features from the datasets to initialize the edge representations e_{ij} . Detailed equations are available in supplementary material. As maintaining edge representations comes with a time and memory cost for the large COLLAB graph, all models use a reduced budget of 27K parameters to fit the GPU memory, and are allowed to train for a maximum of 24 hours for convergence.

Analysis. On both TSP and COLLAB, upgrading isotropic models with edge features significantly boosts performance given the same model parameters (*e.g.* 0.75 vs. 0.64 F1 score on TSP, 50.6% vs. 35.9% Hits@50 on COLLAB for GatedGCN with edge features vs. the isotropic variant). Maintaining explicit edge representations across layers further improves F1 score for TSP, especially when initializing the edge representations with euclidean distances between nodes (*e.g.* 0.78 vs. 0.67 F1 score for GAT-E vs. standard GAT). On COLLAB, adding explicit edge representations and inputs degrades performance, suggesting that the features (collaboration frequency and year) are not useful for the link prediction task (*e.g.* 47.2 vs. 51.5 Hits@50 for GatedGCN-E vs. GatedGCN). As suggested by [87], it would be interesting to treat COLLAB as a multi-graph with temporal edges, motivating the development of task-specific anisotropic edge representations beyond generic attention and gating mechanisms.

5 Conclusion

We introduce a new benchmarking framework to rigorously evaluate the performance of graph neural networks on medium-scale datasets, and demonstrate its usefulness for analyzing message-passing based and theoretically expressive GNNs. As we make our code open-source, easy to use and reproducible, we hope the community will find this project useful to prototype the latest GNN architectures and track progress in graph representation learning.

Broader Impact

This paper proposes a reproducible benchmarking infrastructure that can fairly and rigorously evaluate graph neural network (GNN) architectures, and track progress in graph representation learning. Our framework is likely to drive the development of general-purpose and theoretically driven GNN models which may be deployed in a variety of downstream applications. We briefly discuss positive use cases and possible negative outcomes in this section.

Better GNN architectures. Graphs are met in a wide range of data-driven problems, and GNNs can be used to tackle them: Social media and e-commerce platforms are using GNNs to improve content recommendation and advertising [91, 94]. GNNs are also driving improvements in content quality and inclusivity of these platforms, *e.g.* monitoring hate speech or fake news spread [65]. Similarly, real-time optimization problems which are modelled by interaction graphs make use of GNNs as their backbone, *e.g.* scheduling of processor chips and power units in hardware systems [56, 21]. GNNs are also driving advancements for complex and high-impact problems in drug discovery [70], circuit design [62], neuroscience [32], and genomics [29].

Conversely, the same architectures which lead to positive outcomes may also be used for malicious purposes, especially in social networks and e-commerce: Models monitoring the spread of fake news could end up helping bad actors in designing adversarial strategies for spreading counterfeit content, or for manipulating behaviour based on network effects. Increased personalization of social media and e-commerce platforms has raised important policy questions regarding the collection, ownership and storage of highly sensitive and personal user information.

New benchmarking frameworks. The act of developing new benchmarks often sets precedence and drives the directions of research in particular communities [72, 83, 7]. Thus, community-driven benchmarks must progress and evolve to reflect the best practices in the community. Benchmark creators must be wary about not letting their frameworks be anchors which weigh a field down, and be open to suggestions and contributions by the broader community.

Collecting and preparing graph datasets also comes with many challenges and arbitrary choice [87]. For example, the datasets used for benchmarking may push for research in favor of specific domains

and applications, or contain biases which disadvantage particular communities. We would encourage users of our benchmark to understand the limitations of current graph machine learning datasets and consider the negative outcomes arising from data-driven systems in real-world scenarios. Ultimately, we believe that questions surrounding personal data and digital privacy are important considerations from both technical as well as public policy standpoints³.

Acknowledgments

XB is supported by NRF Fellowship NRFF2017-10.

References

- [1] Emmanuel Abbe. Community detection and stochastic block models: recent developments. *The Journal of Machine Learning Research*, 18(1):6446–6531, 2017.
- [2] Radhakrishna Achanta, Appu Shaji, Kevin Smith, Aurelien Lucchi, Pascal Fua, and Sabine Süsstrunk. Slic superpixels compared to state-of-the-art superpixel methods. *IEEE transactions on pattern analysis and machine intelligence*, 34(11):2274–2282, 2012.
- [3] Radhakrishna Achanta, Appu Shaji, Kevin Smith, Aurelien Lucchi, Pascal Fua, and Sabine Süsstrunk. Slic superpixels compared to state-of-the-art superpixel methods. *IEEE Trans. Pattern Anal. Mach. Intell.*, 34(11):2274–2282, November 2012.
- [4] David Applegate, Ribert Bixby, Vasek Chvatal, and William Cook. Concorde tsp solver, 2006.
- [5] Jimmy Lei Ba, Jamie Ryan Kiros, and Geoffrey E Hinton. Layer normalization. *NeurIPS workshop on Deep Learning*, 2016.
- [6] Dzmitry Bahdanau, Kyunghyun Cho, and Yoshua Bengio. Neural machine translation by jointly learning to align and translate. *arXiv preprint arXiv:1409.0473*, 2014.
- [7] Andrei Barbu, David Mayo, Julian Alverio, William Luo, Christopher Wang, Dan Gutfreund, Josh Tenenbaum, and Boris Katz. Objectnet: A large-scale bias-controlled dataset for pushing the limits of object recognition models. In *Advances in Neural Information Processing Systems*, pages 9448–9458, 2019.
- [8] Peter Battaglia, Razvan Pascanu, Matthew Lai, Danilo Jimenez Rezende, et al. Interaction networks for learning about objects, relations and physics. In *Advances in neural information processing systems*, pages 4502–4510, 2016.
- [9] Mikhail Belkin and Partha Niyogi. Laplacian eigenmaps for dimensionality reduction and data representation. *Neural computation*, 15(6):1373–1396, 2003.
- [10] Yoshua Bengio, Andrea Lodi, and Antoine Prouvost. Machine learning for combinatorial optimization: a methodological tour d’horizon. *arXiv preprint arXiv:1811.06128*, 2018.
- [11] Xavier Bresson and Thomas Laurent. Residual gated graph convnets. *arXiv preprint arXiv:1711.07553*, 2017.
- [12] Xavier Bresson and Thomas Laurent. A two-step graph convolutional decoder for molecule generation. In *NeurIPS Workshop on Machine Learning and the Physical Sciences*, 2019.
- [13] Marc Brockschmidt. Gnn-film: Graph neural networks with feature-wise linear modulation. *arXiv preprint arXiv:1906.12192*, 2019.
- [14] Joan Bruna, Wojciech Zaremba, Arthur Szlam, and Yann LeCun. Spectral networks and locally connected networks on graphs. *arXiv preprint arXiv:1312.6203*, 2013.
- [15] Ines Chami, Sami Abu-El-Haija, Bryan Perozzi, Christopher Ré, and Kevin Murphy. Machine learning on graphs: A model and comprehensive taxonomy. *arXiv preprint arXiv:2005.03675*, 2020.
- [16] Ines Chami, Adva Wolf, Da-Cheng Juan, Frederic Sala, Sujith Ravi, and Christopher Ré. Low-dimensional hyperbolic knowledge graph embeddings. *arXiv preprint arXiv:2005.00545*, 2020.

³<https://www.montrealdeclaration-responsibleai.com/>

- [17] Ting Chen, Song Bian, and Yizhou Sun. Are powerful graph neural nets necessary? a dissection on graph classification, 2019.
- [18] Zhengdao Chen, Soledad Villar, Lei Chen, and Joan Bruna. On the equivalence between graph isomorphism testing and function approximation with gnns. In *Advances in Neural Information Processing Systems*, pages 15868–15876, 2019.
- [19] Wei-Lin Chiang, Xuanqing Liu, Si Si, Yang Li, Samy Bengio, and Cho-Jui Hsieh. Cluster-gcn: An efficient algorithm for training deep and large graph convolutional networks. In *Proceedings of the 25th ACM SIGKDD International Conference on Knowledge Discovery & Data Mining*, pages 257–266, 2019.
- [20] Miles D Cranmer, Rui Xu, Peter Battaglia, and Shirley Ho. Learning symbolic physics with graph networks. *arXiv preprint arXiv:1909.05862*, 2019.
- [21] Jeffrey Dean. The deep learning revolution and its implications for computer architecture and chip design. In *2020 IEEE International Solid-State Circuits Conference-(ISSCC)*, pages 8–14. IEEE, 2020.
- [22] Michaël Defferrard, Xavier Bresson, and Pierre Vandergheynst. Convolutional neural networks on graphs with fast localized spectral filtering. In *Advances in Neural Information Processing Systems* 29, pages 3844–3852. 2016.
- [23] Arthur P Dempster, Nan M Laird, and Donald B Rubin. Maximum likelihood from incomplete data via the em algorithm. *Journal of the Royal Statistical Society: Series B (Methodological)*, 39(1):1–22, 1977.
- [24] J. Deng, W. Dong, R. Socher, L.-J. Li, K. Li, and L. Fei-Fei. ImageNet: A Large-Scale Hierarchical Image Database. In *CVPR09*, 2009.
- [25] David K Duvenaud, Dougal Maclaurin, Jorge Iparraguirre, Rafael Bombarell, Timothy Hirzel, Alán Aspuru-Guzik, and Ryan P Adams. Convolutional networks on graphs for learning molecular fingerprints. In *Advances in neural information processing systems*, pages 2224–2232, 2015.
- [26] Federico Errica, Marco Podda, Davide Bacciu, and Alessio Micheli. A fair comparison of graph neural networks for graph classification, 2019.
- [27] Matthias Fey and Jan Eric Lenssen. Fast graph representation learning with pytorch geometric. *ICLR Workshop on Representation Learning on Graphs and Manifolds*, 2019.
- [28] Charless Fowlkes, Serge Belongie, Fan Chung, and Jitendra Malik. Spectral grouping using the nystrom method. *IEEE transactions on pattern analysis and machine intelligence*, 26(2):214–225, 2004.
- [29] Pablo Gainza, Freyr Sverrisson, Frederico Monti, Emanuele Rodola, D Boscaini, MM Bronstein, and BE Correia. Deciphering interaction fingerprints from protein molecular surfaces using geometric deep learning. *Nature Methods*, 17(2):184–192, 2020.
- [30] Lise Getoor. Link-based classification. In *Advanced methods for knowledge discovery from complex data*, pages 189–207. Springer, 2005.
- [31] Justin Gilmer, Samuel S Schoenholz, Patrick F Riley, Oriol Vinyals, and George E Dahl. Neural message passing for quantum chemistry. In *Proceedings of the 34th International Conference on Machine Learning-Volume 70*, pages 1263–1272. JMLR. org, 2017.
- [32] Alessandra Griffo, Benjamin Ricaud, Kirell Benzi, Xavier Bresson, Alessandro Daducci, Pierre Vandergheynst, Jean-Philippe Thiran, and Patric Hagmann. Transient networks of spatio-temporal connectivity map communication pathways in brain functional systems. *NeuroImage*, 155:490–502, 2017.
- [33] Will Hamilton, Zhitaoying, and Jure Leskovec. Inductive representation learning on large graphs. In *Advances in Neural Information Processing Systems*, pages 1024–1034, 2017.
- [34] Kaiming He, Xiangyu Zhang, Shaoqing Ren, and Jian Sun. Deep residual learning for image recognition. In *The IEEE Conference on Computer Vision and Pattern Recognition (CVPR)*, June 2016.
- [35] NT Hoang and Takanori Maehara. Revisiting graph neural networks: All we have is low-pass filters. *ArXiv*, abs/1905.09550, 2019.

- [36] Sergey Ioffe and Christian Szegedy. Batch normalization: Accelerating deep network training by reducing internal covariate shift. *arXiv preprint arXiv:1502.03167*, 2015.
- [37] John J Irwin, Teague Sterling, Michael M Mysinger, Erin S Bolstad, and Ryan G Coleman. Zinc: a free tool to discover chemistry for biology. *Journal of chemical information and modeling*, 52(7):1757–1768, 2012.
- [38] Zhihao Jia, Sina Lin, Rex Ying, Jiaxuan You, Jure Leskovec, and Alex Aiken. Redundancy-free computation graphs for graph neural networks. *arXiv preprint arXiv:1906.03707*, 2019.
- [39] Wengong Jin, Regina Barzilay, and Tommi Jaakkola. Junction tree variational autoencoder for molecular graph generation. *arXiv preprint arXiv:1802.04364*, 2018.
- [40] Chaitanya K Joshi, Thomas Laurent, and Xavier Bresson. An efficient graph convolutional network technique for the travelling salesman problem. *arXiv preprint arXiv:1906.01227*, 2019.
- [41] Kristian Kersting, Nils M. Kriege, Christopher Morris, Petra Mutzel, and Marion Neumann. Benchmark data sets for graph kernels, 2020.
- [42] Elias Khalil, Hanjun Dai, Yuyu Zhang, Bistra Dilkina, and Le Song. Learning combinatorial optimization algorithms over graphs. In *Advances in Neural Information Processing Systems*, pages 6348–6358, 2017.
- [43] Diederik P Kingma and Jimmy Ba. Adam: A method for stochastic optimization. *arXiv preprint arXiv:1412.6980*, 2014.
- [44] Thomas N. Kipf and Max Welling. Semi-supervised classification with graph convolutional networks. In *International Conference on Learning Representations (ICLR)*, 2017.
- [45] Boris Knyazev, Graham W Taylor, and Mohamed R Amer. Understanding attention and generalization in graph neural networks. *arXiv preprint arXiv:1905.02850*, 2019.
- [46] Wouter Kool, Herke van Hoof, and Max Welling. Attention, learn to solve routing problems! In *International Conference on Learning Representations*, 2019.
- [47] Alex Krizhevsky et al. Learning multiple layers of features from tiny images. 2009.
- [48] Alex Krizhevsky, Ilya Sutskever, and Geoffrey E. Hinton. Imagenet classification with deep convolutional neural networks. In *Advances in Neural Information Processing Systems 25: 26th Annual Conference on Neural Information Processing Systems 2012.*, pages 1106–1114, 2012.
- [49] Yann LeCun, Yoshua Bengio, et al. Convolutional networks for images, speech, and time series. 1995.
- [50] Yann LeCun, Léon Bottou, Yoshua Bengio, and Patrick Haffner. Gradient-based learning applied to document recognition. *Proceedings of the IEEE*, 86(11):2278–2324, 1998.
- [51] Guohao Li, Matthias Müller, Guocheng Qian, Itzel C Delgadillo, Abdullellah Abualshour, Ali Thabet, and Bernard Ghanem. Deepgcns: Making gcns go as deep as cnns. *International Conference on Computer Vision*, 2019.
- [52] Zhuwen Li, Qifeng Chen, and Vladlen Koltun. Combinatorial optimization with graph convolutional networks and guided tree search. In *Advances in Neural Information Processing Systems*, pages 539–548, 2018.
- [53] Sharon L Lohr. *Sampling: design and analysis*. Nelson Education, 2009.
- [54] Enxhell Luzhnica, Ben Day, and Pietro Liò. On graph classification networks, datasets and baselines. *arXiv preprint arXiv:1905.04682*, 2019.
- [55] Jitendra Malik. Technical perspective: What led computer vision to deep learning? *Commun. ACM*, 60(6):82–83, May 2017.
- [56] Hongzi Mao, Malte Schwarzkopf, Shaileshh Bojja Venkatakrishnan, Zili Meng, and Mohammad Alizadeh. Learning scheduling algorithms for data processing clusters. In *Proceedings of the ACM Special Interest Group on Data Communication*, pages 270–288. 2019.
- [57] Diego Marcheggiani and Ivan Titov. Encoding sentences with graph convolutional networks for semantic role labeling. *arXiv preprint arXiv:1703.04826*, 2017.
- [58] Haggai Maron, Heli Ben-Hamu, Hadar Serviansky, and Yaron Lipman. Provably powerful graph networks. In *Advances in Neural Information Processing Systems*, pages 2153–2164, 2019.

- [59] Haggai Maron, Heli Ben-Hamu, Nadav Shamir, and Yaron Lipman. Invariant and equivariant graph networks. *International Conference on Learning Representations*, 2019.
- [60] Haggai Maron, Ethan Fetaya, Nimrod Segol, and Yaron Lipman. On the universality of invariant networks. *International Conference on Machine Learning*, 2019.
- [61] Andrew Kachites McCallum, Kamal Nigam, Jason Rennie, and Kristie Seymore. Automating the construction of internet portals with machine learning. *Information Retrieval*, 3(2):127–163, 2000.
- [62] Azalia Mirhoseini, Anna Goldie, Mustafa Yazgan, Joe Jiang, Ebrahim Songhori, Shen Wang, Young-Joon Lee, Eric Johnson, Omkar Pathak, Sungmin Bae, et al. Chip placement with deep reinforcement learning. *arXiv preprint arXiv:2004.10746*, 2020.
- [63] Federico Monti, Davide Boscaini, Jonathan Masci, Emanuele Rodola, Jan Svoboda, and Michael M. Bronstein. Geometric deep learning on graphs and manifolds using mixture model cnns. *2017 IEEE Conference on Computer Vision and Pattern Recognition (CVPR)*, Jul 2017.
- [64] Federico Monti, Michael Bronstein, and Xavier Bresson. Geometric matrix completion with recurrent multi-graph neural networks. In *Advances in Neural Information Processing Systems*, pages 3697–3707, 2017.
- [65] Federico Monti, Fabrizio Frasca, Davide Eynard, Damon Mannion, and Michael M Bronstein. Fake news detection on social media using geometric deep learning. *arXiv preprint arXiv:1902.06673*, 2019.
- [66] Christopher Morris, Martin Ritzert, Matthias Fey, William L Hamilton, Jan Eric Lenssen, Gaurav Rattan, and Martin Grohe. Weisfeiler and leman go neural: Higher-order graph neural networks. In *Proceedings of the AAAI Conference on Artificial Intelligence*, volume 33, pages 4602–4609, 2019.
- [67] Ryan Murphy, Balasubramaniam Srinivasan, Vinayak Rao, and Bruno Ribeiro. Relational pooling for graph representations. In *International Conference on Machine Learning*, pages 4663–4673, 2019.
- [68] Adam Paszke, Sam Gross, Francisco Massa, Adam Lerer, James Bradbury, Gregory Chanan, Trevor Killeen, Zeming Lin, Natalia Gimelshein, Luca Antiga, Alban Desmaison, Andreas Köpf, Edward Yang, Zach DeVito, Martin Raison, Alykhan Tejani, Sasank Chilamkurthy, Benoit Steiner, Lu Fang, Junjie Bai, and Soumith Chintala. Pytorch: An imperative style, high-performance deep learning library, 2019.
- [69] Pietro Perona and Jitendra Malik. Scale-space and edge detection using anisotropic diffusion. *IEEE Transactions on pattern analysis and machine intelligence*, 12(7):629–639, 1990.
- [70] Maithra Raghu and Eric Schmidt. A survey of deep learning for scientific discovery. *arXiv preprint arXiv:2003.11755*, 2020.
- [71] Emanuele Rossi, Fabrizio Frasca, Ben Chamberlain, Davide Eynard, Michael Bronstein, and Federico Monti. Sign: Scalable inception graph neural networks. *arXiv preprint arXiv:2004.11198*, 2020.
- [72] Olga Russakovsky, Jia Deng, Hao Su, Jonathan Krause, Sanjeev Satheesh, Sean Ma, Zhiheng Huang, Andrej Karpathy, Aditya Khosla, Michael Bernstein, et al. Imagenet large scale visual recognition challenge. *International journal of computer vision*, 115(3):211–252, 2015.
- [73] Alvaro Sanchez-Gonzalez, Jonathan Godwin, Tobias Pfaff, Rex Ying, Jure Leskovec, and Peter W Battaglia. Learning to simulate complex physics with graph networks. *arXiv preprint arXiv:2002.09405*, 2020.
- [74] Alvaro Sanchez-Gonzalez, Nicolas Heess, Jost Tobias Springenberg, Josh Merel, Martin Riedmiller, Raia Hadsell, and Peter Battaglia. Graph networks as learnable physics engines for inference and control. In *International Conference on Machine Learning*, pages 4470–4479, 2018.
- [75] F. Scarselli, M. Gori, A. Tsoi, M. Hagenbuchner, and G. Monfardini. The Graph Neural Network Model. *IEEE Transactions on Neural Networks*, 20(1):61–80, 2009.
- [76] Michael Schlichtkrull, Thomas N Kipf, Peter Bloem, Rianne Van Den Berg, Ivan Titov, and Max Welling. Modeling relational data with graph convolutional networks. In *European Semantic Web Conference*, pages 593–607. Springer, 2018.

- [77] Balasubramaniam Srinivasan and Bruno Ribeiro. On the equivalence between node embeddings and structural graph representations. *International Conference on Learning Representations*, 2020.
- [78] Sainbayar Sukhbaatar, arthur szlam, and Rob Fergus. Learning multiagent communication with backpropagation. In D. D. Lee, M. Sugiyama, U. V. Luxburg, I. Guyon, and R. Garnett, editors, *Advances in Neural Information Processing Systems 29*, pages 2244–2252. 2016.
- [79] Ashish Vaswani, Noam Shazeer, Niki Parmar, Jakob Uszkoreit, Llion Jones, Aidan N Gomez, Łukasz Kaiser, and Illia Polosukhin. Attention is all you need. In *Advances in neural information processing systems*, pages 5998–6008, 2017.
- [80] Petar Veličković, Guillem Cucurull, Arantxa Casanova, Adriana Romero, Pietro Liò, and Yoshua Bengio. Graph Attention Networks. *International Conference on Learning Representations*, 2018.
- [81] Oriol Vinyals, Meire Fortunato, and Navdeep Jaitly. Pointer networks. In *Advances in Neural Information Processing Systems*, pages 2692–2700, 2015.
- [82] Ulrike Von Luxburg. A tutorial on spectral clustering. *Statistics and computing*, 17(4):395–416, 2007.
- [83] Alex Wang, Yada Pruksachatkun, Nikita Nangia, Amanpreet Singh, Julian Michael, Felix Hill, Omer Levy, and Samuel Bowman. Superglue: A stickier benchmark for general-purpose language understanding systems. In *Advances in Neural Information Processing Systems*, pages 3261–3275, 2019.
- [84] Kuansan Wang, Zhihong Shen, Chiyuan Huang, Chieh-Han Wu, Yuxiao Dong, and Anshul Kanakia. Microsoft academic graph: When experts are not enough. *Quantitative Science Studies*, 1(1):396–413, 2020.
- [85] Minjie Wang, Lingfan Yu, Da Zheng, Quan Gan, Yu Gai, Zihao Ye, Mufei Li, Jinjing Zhou, Qi Huang, Chao Ma, Ziyue Huang, Qipeng Guo, Hao Zhang, Haibin Lin, Junbo Zhao, Jinyang Li, Alexander J Smola, and Zheng Zhang. Deep graph library: Towards efficient and scalable deep learning on graphs. *ICLR Workshop on Representation Learning on Graphs and Manifolds*, 2019.
- [86] Lukas M Weber, Wouter Saelens, Robrecht Cannoodt, Charlotte Soneson, Alexander Hapfelmeier, Paul P Gardner, Anne-Laure Boulesteix, Yvan Saeys, and Mark D Robinson. Essential guidelines for computational method benchmarking. *Genome biology*, 20(1):125, 2019.
- [87] Marinka Zitnik Yuxiao Dong Hongyu Ren Bowen Liu Michele Catasta Jure Leskovec Weihua Hu, Matthias Fey. Open graph benchmark: Datasets for machine learning on graphs. *arXiv preprint arXiv:2005.00687*, 2020.
- [88] Boris Weisfeiler and Andrei A Lehman. A reduction of a graph to a canonical form and an algebra arising during this reduction. *Nauchno-Tekhnicheskaya Informatsia*, 2(9):12–16, 1968.
- [89] Keyulu Xu, Weihua Hu, Jure Leskovec, and Stefanie Jegelka. How powerful are graph neural networks? In *International Conference on Learning Representations*, 2019.
- [90] Keyulu Xu, Chengtao Li, Yonglong Tian, Tomohiro Sonobe, Ken-ichi Kawarabayashi, and Stefanie Jegelka. Representation learning on graphs with jumping knowledge networks. *arXiv preprint arXiv:1806.03536*, 2018.
- [91] Rex Ying, Ruining He, Kaifeng Chen, Pong Eksombatchai, William L Hamilton, and Jure Leskovec. Graph convolutional neural networks for web-scale recommender systems. In *Proceedings of the 24th ACM SIGKDD International Conference on Knowledge Discovery & Data Mining*, pages 974–983, 2018.
- [92] Jiaxuan You, Bowen Liu, Zhitao Ying, Vijay Pande, and Jure Leskovec. Graph convolutional policy network for goal-directed molecular graph generation. In *Advances in neural information processing systems*, pages 6410–6421, 2018.
- [93] Jiaxuan You, Rex Ying, and Jure Leskovec. Position-aware graph neural networks. *International Conference on Machine Learning*, 2019.
- [94] Rong Zhu, Kun Zhao, Hongxia Yang, Wei Lin, Chang Zhou, Baole Ai, Yong Li, and Jingren Zhou. Aligraph: a comprehensive graph neural network platform. *Proceedings of the VLDB Endowment*, 12(12):2094–2105, 2019.

A Datasets and experimental details

We now provide additional information related to the preparation of the datasets described in Section 2.3 of the proposed benchmarking framework, as well as the corresponding experimental setting for training and performance metrics.

A.1 Node Classification with SBM Datasets

The SBM datasets consider node-level tasks of graph pattern recognition [75] – PATTERN and semi-supervised graph clustering – CLUSTER. The graphs are generated with the Stochastic Block Model (SBM) [1], which is widely used to model communities in social networks by modulating the intra- and extra-communities connections, thereby controlling the difficulty of the task. A SBM is a random graph which assigns communities to each node as follows: any two vertices are connected with the probability p if they belong to the same community, or they are connected with the probability q if they belong to different communities (the value of q acts as the noise level).

PATTERN: The graph pattern recognition task, presented in [75], aims at finding a fixed graph pattern P embedded in larger graphs G of variable sizes. For all data, we generate graphs G with 5 communities with sizes randomly selected between [5, 35]. The SBM of each community is $p = 0.5, q = 0.35$, and the node features on G are generated with a uniform random distribution with a vocabulary of size 3, *i.e.* $\{0, 1, 2\}$. We randomly generate 100 patterns P composed of 20 nodes with intra-probability $p_P = 0.5$ and extra-probability $q_P = 0.5$ (*i.e.*, 50% of nodes in P are connected to G). The node features for P are also generated as a random signal with values $\{0, 1, 2\}$. The graphs are of sizes 44-188 nodes. The output node labels have value 1 if the node belongs to P and value 0 if it is in G .

CLUSTER: For the semi-supervised clustering task, we generate 6 SBM clusters with sizes randomly selected between [5, 35] and probabilities $p = 0.55, q = 0.25$. The graphs are of sizes 40-190 nodes. Each node can take an input feature value in $\{0, 1, 2, \dots, 6\}$. If the value is 1, the node belongs to class 0, value 2 corresponds to class 1, ..., value 6 corresponds to class 5. Otherwise, if the value is 0, the class of the node is unknown and will be inferred by the GNN. There is only one labelled node that is randomly assigned to each community and most node features are set to 0. The output node labels are defined as the community/cluster class labels.

Splitting. The PATTERN dataset has 10000 train/2000 validation/2000 test graphs and CLUSTER dataset has 10000 train/1000 validation/1000 test graphs. We save the generated splits and use the same sets in all models for fair comparison.

Training. As presented in the standard experimental protocol in Section 3, we use Adam optimizer with a learning rate decay strategy. For all GNNs, an initial learning rate is set to 1×10^{-3} , the reduce factor is 0.5, the patience value is 5, and the stopping learning rate is 1×10^{-5} .

Performance Measure. The performance measure is the average node-level accuracy weighted with respect to the class sizes.

A.2 Graph Classification with Super-pixel Datasets

The super-pixels datasets test graph classification using the popular MNIST and CIFAR10 image classification datasets. Our main motivation to use these datasets is as sanity-checks: we expect most GNNs to perform close to 100% for MNIST and well enough for CIFAR10.

The original MNIST and CIFAR10 images are converted to graphs using super-pixels. Super-pixels represent small regions of homogeneous intensity in images, and can be extracted with the SLIC technique [3]. We use SLIC super-pixels from [45]⁴. For each sample, we build a k -nearest neighbor adjacency matrix with

$$W_{ij}^{k\text{-NN}} = \exp\left(-\frac{\|x_i - x_j\|^2}{\sigma_x^2}\right), \quad (9)$$

where x_i, x_j are the 2-D coordinates of super-pixels i, j , and σ_x is the scale parameter defined as the averaged distance x_k of the k nearest neighbors for each node. We use $k = 8$ for both MNIST and CIFAR10, whereas the maximum number of super-pixels (nodes) are 75 and 150 for MNIST and

⁴https://github.com/bknyaz/graph_attention_pool

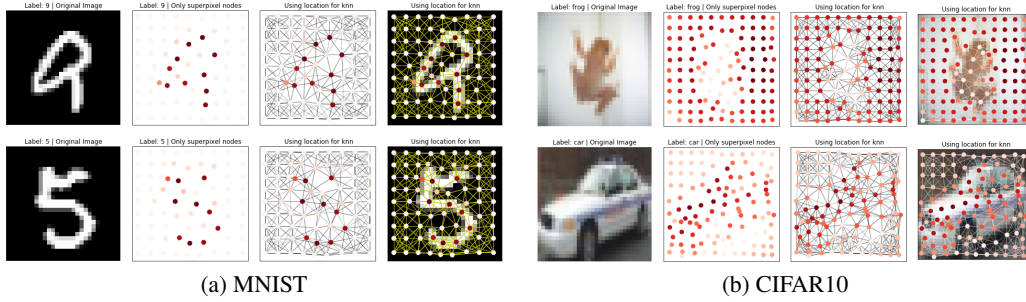


Figure 1: Sample images and their superpixel graphs. The graphs of SLIC superpixels (at most 75 nodes for MNIST and 150 nodes for CIFAR10) are 8-nearest neighbor graphs in the Euclidean space and node colors denote the mean pixel intensities.

CIFAR10, respectively. The resultant graphs are of sizes 40-75 nodes for MNIST and 85-150 nodes for CIFAR10. Figure 1 presents visualizations of the super-pixel graphs.

Splitting. We use the standard splits of MNIST and CIFAR10. MNIST has 55000 train/5000 validation/10000 test graphs and CIFAR10 has 45000 train/5000 validation/10000 test graphs. The 5000 graphs for validation set are randomly sampled from the training set and the same splits are used for every GNN.

Training. The learning decay rate strategy is adopted with an initial learning rate of 1×10^{-3} , reduce factor 0.5, patience value 10, and the stopping learning rate 1×10^{-5} for all GNNs, except for 3WLGNN and RingGNN where we experienced a difficulty in training, leading us to slightly adjust their learning rate schedule hyperparameters. For both 3WLGNN and RingGNN, the patience value is changed to 5. For RingGNN, the initial learning rate is changed to 1×10^{-4} and the stopping learning rate is changed to 1×10^{-6} .

Performance Measure. The classification accuracy between the predicted and groundtruth label for each graph is the performance measure.

A.3 Edge Classification/Link Prediction with TSP Dataset

Leveraging machine learning for solving NP-hard combinatorial optimization problems (COPs) has been the focus of intense research in recent years [81, 10]. Recently proposed learning-driven solvers for COPs [42, 52, 46] combine GNNs with classical search to predict approximate solutions directly from problem instances (represented as graphs). Consider the intensively studied Travelling Salesman Problem (TSP), which asks the following question: “Given a list of cities and the distances between each pair of cities, what is the shortest possible route that visits each city and returns to the origin city?” Formally, given a 2D Euclidean graph, one needs to find an optimal sequence of nodes, called a tour, with minimal total edge weights (tour length). TSP’s *multi-scale* nature makes it a challenging graph task which requires reasoning about both local node neighborhoods as well as global graph structure.

For our experiments with TSP, we follow the learning-based approach to COPs described in [52, 40], where a GNN is the backbone architecture for assigning probabilities to each edge as belonging/not belonging to the predicted solution set. The probabilities are then converted into discrete decisions through graph search techniques. Each instance is a graph of n node locations sampled uniformly in the unit square $S = \{x_i\}_{i=1}^n$ and $x_i \in [0, 1]^2$. We generate problems of varying size and complexity by uniformly sampling the number of nodes $n \in [50, 500]$ for each instance.

In order to isolate the impact of the backbone GNN architectures from the search component, we pose TSP as a binary edge classification task, with the groundtruth value for each edge belonging to the TSP tour given by Concorde [4]. For scaling to large instances, we use sparse $k = 25$ nearest neighbor graphs instead of full graphs, following [42]. See Figure 2 for sample TSP instances of various sizes.

Splitting. TSP has 10000 train, 1000 validation and 1000 test graphs.

Training. All GNNs use a consistent learning rate strategy: an initial learning rate is set to 1×10^{-3} ,

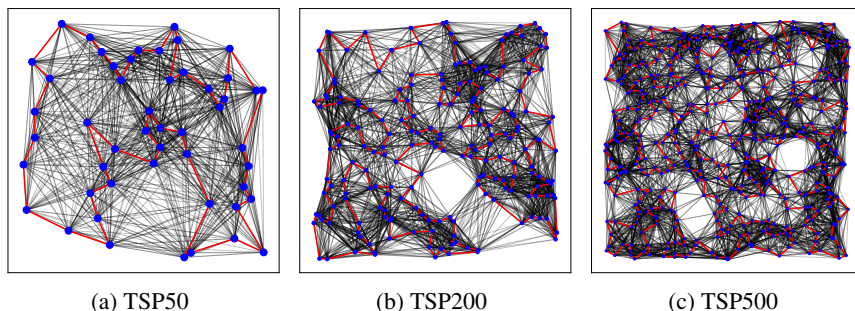


Figure 2: Sample graphs from the TSP dataset. Nodes are colored blue and edges on the groundtruth TSP tours are colored red.

the reduce factor is 0.5, the patience value is 10, and the stopping learning rate is 1×10^{-5} .

Performance Measure. Given the high class imbalance, *i.e.*, only the edges in the TSP tour have positive label, we use the F1 score for the positive class as our performance measure.

Non-learned Baseline. In addition to reporting performance of GNNs, we compare with a simple k -nearest neighbor heuristic baseline, defined as follows: Predict true for the edges corresponding to the k nearest neighbors of each node, and false for all other edges. We set $k = 2$ for optimal performance. Comparing GNNs to the non-learned baseline tells us whether models learn something more sophisticated than identifying a node’s nearest neighbors.

A.4 Link Prediction with COLLAB dataset

COLLAB is a link prediction dataset proposed by OGB [87] corresponding to a collaboration network between approximately 235K scientists, indexed by Microsoft Academic Graph [84]. Nodes represent scientists and edges denote collaborations between them. For node features, OGB provides 128-dimensional vectors, obtained by averaging the word embeddings of a scientist’s papers. The year and number of co-authored papers in a given year are concatenated to form edge features. The graph can also be viewed as a dynamic multi-graph, since two nodes may have multiple temporal edges between if they collaborate over multiple years.

Through the introduction of the COLLAB dataset, we additionally want to demonstrate that our benchmarking infrastructure is complementary to the OGB initiative, and is well-suited to integrate current and future OGB dataset and evaluation protocols.

Splitting. We use the realistic training, validation and test edge splits provided by OGB. Specifically, they use collaborations until 2017 as training edges, those in 2018 as validation edges, and those in 2019 as test edges.

Training. All GNNs use a consistent learning rate strategy: an initial learning rate is set to 1×10^{-3} , the reduce factor is 0.5, the patience value is 10, and the stopping learning rate is 1×10^{-5} .

Performance Measure. We use the evaluator provided by OGB, which aims to measure a model’s ability to predict future collaboration relationships given past collaborations. Specifically, they rank each true collaboration among a set of 100,000 randomly-sampled negative collaborations, and count the ratio of positive edges that are ranked at K -place or above (Hits@ K). They suggested using $K = 10$ through their preliminary experiments, but we found $K = 50$ to better for statistically separating the performance of GNNs.

Matrix Factorization Baseline. In addition to GNNs, we report performance for a simple matrix factorization baseline [87], which trains 256-dimensional embeddings for each of the 235K nodes. Comparing GNNs to matrix factorization tells us whether models leverage node features in addition to graph structure, as matrix factorization can be thought of as feature-agnostic.

A.5 Graph Regression with ZINC dataset

We use a subset (12K) of ZINC molecular graphs (250K) dataset [37] to regress a molecular property known as the constrained solubility. For each molecular graph, the node features are the types of heavy atoms and the edge features are the types of bonds between them.

Splitting. ZINC has 10000 train, 1000 validation and 1000 test graphs.

Training. For the learning rate strategy across all GNNs, an initial learning rate is set to 1×10^{-3} , the reduce factor is 0.5, and the stopping learning rate is 1×10^{-5} . The patience value is 5 for 3WLGNN and RingGNN, and 10 for all other GNNs.

Performance Measure. The performance measure is the mean absolute error (MAE) between the predicted and the groundtruth constrained solubility for each molecular graph.

A.6 Graph Classification and Isomorphism Testing with CSL dataset

The Circular Skip Link dataset is a symmetric graph dataset introduced in [67] to test the expressivity of GNNs. Each CSL graph is a 4-regular graph with edges connected to form a cycle and containing skip-links between nodes. Formally, it is denoted by $\mathcal{G}_{N,C}$ where N is the number of nodes and C is the isomorphism class which is the skip-link of the graph. We use the same dataset $\mathcal{G}_{41,C}$ with $C \in \{2, 3, 4, 5, 6, 9, 11, 12, 13, 16\}$. The dataset is class-balanced with 15 graphs for every C resulting in a total of 150 graphs.

Splitting. We perform a 5-fold cross validation split, following [67], which gives 5 sets of train, validation and test data indices in the ratio 3 : 1 : 1. We use stratified sampling to ensure that the class distribution remains the same across splits. The indices are saved and used across all experiments for fair comparisons.

Training. For the learning rate strategy across all GNNs, an initial learning rate is set to 5×10^{-4} , the reduce factor is 0.5, the patience value is 5, and the stopping learning rate is 1×10^{-6} . We train on the 5-fold cross validation with 20 different seeds of initialization, following [18].

Performance Measure. We use graph classification accuracy between the predicted labels and groundtruth labels as our performance measure. The model performance is evaluated on the test split of the 5 folds at every run, and following [67, 18], we report the maximum, minimum, average and the standard deviation of the 100 scores, *i.e.*, 20 runs of 5-folds.

Table 5: Summary statistics of all datasets. Numbers in parentheses of Node features and Edge features are the dimensions.

Dataset	#Graphs	#Classes	Avg. Nodes	Avg. Edges	Node feat. (dim)	Edge feat. (dim)
ZINC	12000	–	23.16	49.83	Atom Type (28)	Bond Type (4)
PATTERN	14000	2	117.47	4749.15	Node Attr (3)	N.A.
CLUSTER	12000	6	117.20	4301.72	Node Attr (7)	N.A.
MNIST	70000	10	70.57	564.53	Pixel+Coord (3)	Node Dist (1)
CIFAR10	60000	10	117.63	941.07	Pixel[RGB]+Coord (5)	Node Dist (1)
TSP	12000	2	275.76	6894.04	Coord (2)	Node Dist (1)
COLLAB	1	–	235868.00	2358104.00	Word Embs (128)	Year & Weight (2)
CSL	150	10	41.00	164.00	N.A.	N.A.
ENZYMES	600	6	32.63	62.14	Node Attr (18)	N.A.
DD	1178	2	284.32	715.66	Node Label (89)	N.A.
PROTEINS	1113	2	39.06	72.82	Node Attr (29)	N.A.

B Graph Neural Networks

This section formally describes our experimental pipeline, illustrated in Figure 3 for **GCNs** and Figure 4 for **WL-GNNs**. In Section B.1, we describe the components of the setup of the GCN class with vanilla GCN [44], GraphSage [33], MoNet [63], GAT [80], and GatedGCN [11], including the input layers, the GNN layers and the task based MLP classifier layers. We also include the description of GIN [89] in this section as this model can be interpreted as a GCN, although it was designed to differentiate non-isomorphic graphs. In Section B.2, we present the GNN layers and the task based MLP classifier layers for the class of WL-GNN models with Ring-GNNs [18] and 3WL-GNNs [58].

B.1 Message-Passing GCNs

B.1.1 Input Layer

Given a graph, we are given node features $\alpha_i \in \mathbb{R}^{a \times 1}$ for each node i and (optionally) edge features $\beta_{ij} \in \mathbb{R}^{b \times 1}$ for each edge connecting node i and node j . The input features α_i and β_{ij} are embedded

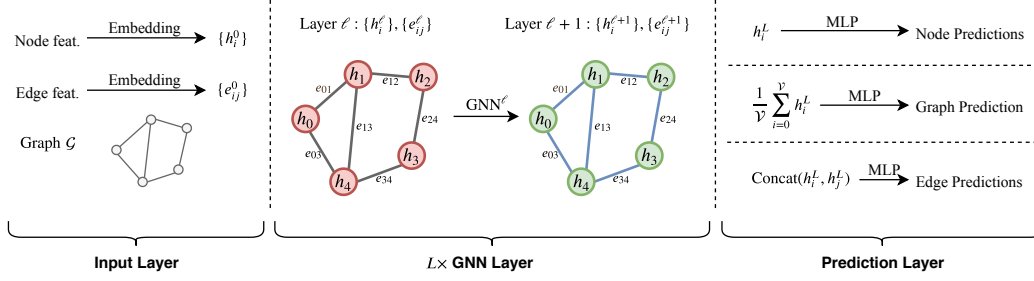


Figure 3: A standard experimental pipeline for GCNs, which embeds the graph node and edge features, performs several GNN layers to compute convolutional features, and finally makes a prediction through a task-specific MLP layer.

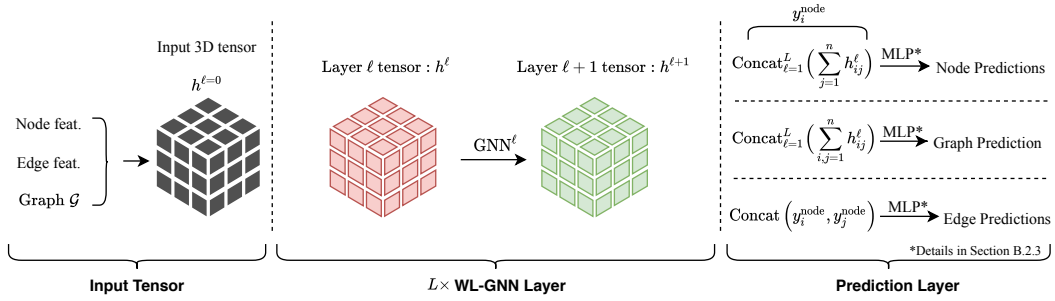


Figure 4: A standard experimental pipeline for WL-GNNs, which inputs to a GNN a graph with all node and edge information (if available) represented by a dense tensor, performs several GNN layer computations over the dense tensor, and finally makes a prediction through a task-specific MLP layer.

to d -dimensional hidden features $h_i^{\ell=0}$ and $e_{ij}^{\ell=0}$ via a simple linear projection before passing them to a graph neural network:

$$h_i^0 = U^0 \alpha_i + u^0 ; \quad e_{ij}^0 = V^0 \beta_{ij} + v^0, \quad (10)$$

where $U^0 \in \mathbb{R}^{d \times a}$, $V^0 \in \mathbb{R}^{d \times b}$ and $u^0, v^0 \in \mathbb{R}^d$. If the input node/edge features are one-hot vectors of discrete variables, then biases u^0, v^0 are not used.

B.1.2 GCN layers

Each GCN layer computes d -dimensional representations for the nodes/edges of the graph through recursive neighborhood diffusion (or message passing), where each graph node gathers features from its neighbors to represent local graph structure. Stacking L GCN layers allows the network to build node representations from the L -hop neighborhood of each node.

Let h_i^ℓ denote the feature vector at layer ℓ associated with node i . The updated features $h_i^{\ell+1}$ at the next layer $\ell + 1$ are obtained by applying non-linear transformations to the central feature vector h_i^ℓ and the feature vectors h_j^ℓ for all nodes j in the neighborhood of node i (defined by the graph structure). This guarantees the transformation to build local reception fields, such as in standard ConvNets for computer vision, and be invariant to both graph size and vertex re-indexing.

Thus, the most generic version of a feature vector $h_i^{\ell+1}$ at vertex i at the next layer in the GNN is:

$$h_i^{\ell+1} = f(h_i^\ell, \{h_j^\ell : j \rightarrow i\}), \quad (11)$$

where $\{j \rightarrow i\}$ denotes the set of neighboring nodes j pointed to node i , which can be replaced by $\{j \in \mathcal{N}_i\}$, the set of neighbors of node i , if the graph is undirected. In other words, a GNN is defined by a mapping f taking as input a vector h_i^ℓ (the feature vector of the center vertex) as well as an un-ordered set of vectors $\{h_j^\ell\}$ (the feature vectors of all neighboring vertices), see Figure 5. The arbitrary choice of the mapping f defines an instantiation of a class of GNNs.

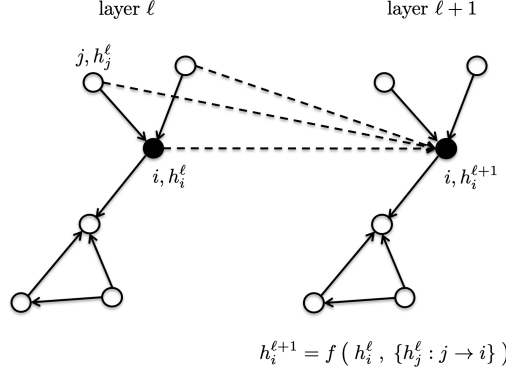


Figure 5: A generic graph neural network layer. Figure adapted from [11].

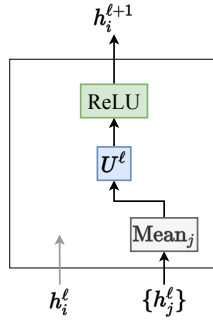


Figure 6: GCN Layer

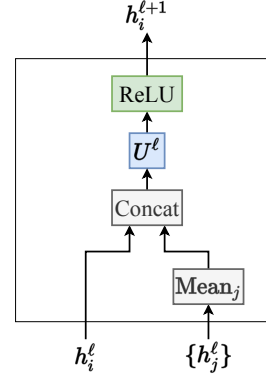


Figure 7: GraphSage Layer

Vanilla Graph ConvNets (GCN) [44] In the simplest formulation of GNNs, Graph ConvNets iteratively update node features via an isotropic averaging operation over the neighborhood node features, *i.e.*,

$$h_i^{\ell+1} = \text{ReLU}\left(U^\ell \text{Mean}_{j \in \mathcal{N}_i} h_j^\ell\right), \quad (12)$$

$$= \text{ReLU}\left(U^\ell \frac{1}{\text{deg}_i} \sum_{j \in \mathcal{N}_i} h_j^\ell\right), \quad (13)$$

where $U^\ell \in \mathbb{R}^{d \times d}$ (a bias is also used, but omitted for clarity purpose), deg_i is the in-degree of node i , see Figure 6. Eq. (12) is called a *convolution* as it is a linear approximation of a localized spectral convolution. Note that it is possible to add the central node features h_i^ℓ in the update (12) by using self-loops or residual connections.

GraphSage [33] GraphSage improves upon the simple GCN model by explicitly incorporating each node's own features from the previous layer in its update equation:

$$\hat{h}_i^{\ell+1} = \text{ReLU}\left(U^\ell \text{Concat}\left(h_i^\ell, \text{Mean}_{j \in \mathcal{N}_i} h_j^\ell\right)\right), \quad (14)$$

where $U^\ell \in \mathbb{R}^{d \times 2d}$, see Figure 7. Observe that the transformation applied to the central node features h_i^ℓ is different to the transformation carried out to the neighborhood features h_j^ℓ . The node features are then projected onto the ℓ_2 -unit ball before being passed to the next layer:

$$h_i^{\ell+1} = \frac{\hat{h}_i^{\ell+1}}{\|\hat{h}_i^{\ell+1}\|_2}. \quad (15)$$

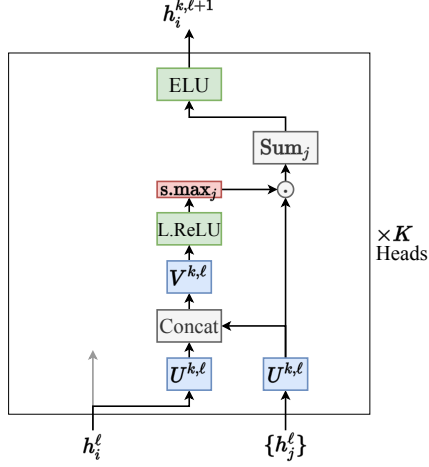


Figure 8: GAT Layer

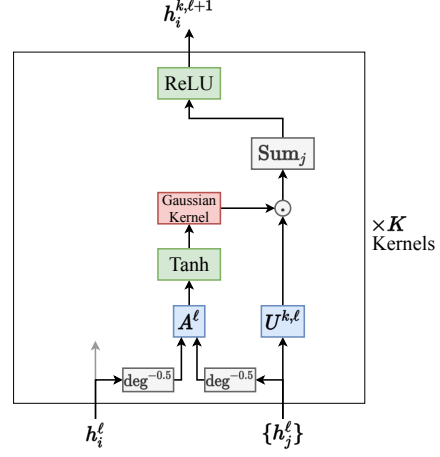


Figure 9: MoNet Layer

The authors also define more sophisticated neighborhood aggregation functions, such as Max-pooling or LSTM aggregators:

$$\hat{h}_i^{\ell+1} = \text{ReLU}\left(U^\ell \text{Concat}\left(h_i^\ell, \text{Max}_{j \in \mathcal{N}_i} \text{ReLU}(V^\ell h_j^\ell)\right)\right), \quad (16)$$

$$\hat{h}_i^{\ell+1} = \text{ReLU}\left(U^\ell \text{Concat}\left(h_i^\ell, \text{LSTM}_{j \in \mathcal{N}_i}^\ell(h_j^\ell)\right)\right), \quad (17)$$

where $V^\ell \in \mathbb{R}^{d \times d}$ and the LSTM^ℓ cell also uses learnable weights. In our experiments, we use the Max-pooling version of GraphSage, Eq.(16).

Graph Attention Network (GAT) [80] GAT uses the attention mechanism of [6] to introduce anisotropy in the neighborhood aggregation function. The network employs a multi-headed architecture to increase the learning capacity, similar to the Transformer [79]. The node update equation is given by:

$$h_i^{\ell+1} = \text{Concat}_{k=1}^K \left(\text{ELU} \left(\sum_{j \in \mathcal{N}_i} e_{ij}^{k,\ell} U^{k,\ell} h_j^\ell \right) \right), \quad (18)$$

where $U^{k,\ell} \in \mathbb{R}^{\frac{d}{K} \times d}$ are the K linear projection heads, and $e_{ij}^{k,\ell}$ are the attention coefficients for each head defined as:

$$e_{ij}^{k,\ell} = \frac{\exp(\hat{e}_{ij}^{k,\ell})}{\sum_{j' \in \mathcal{N}_i} \exp(\hat{e}_{ij'}^{k,\ell})}, \quad (19)$$

$$\hat{e}_{ij}^{k,\ell} = \text{LeakyReLU}\left(V^{k,\ell} \text{Concat}(U^{k,\ell} h_i^\ell, U^{k,\ell} h_j^\ell)\right), \quad (20)$$

where $V^{k,\ell} \in \mathbb{R}^{\frac{2d}{K}}$, see Figure 8. GAT learns a mean over each node's neighborhood features sparsely weighted by the importance of each neighbor.

MoNet [63] The MoNet model introduces a general architecture to learn on graphs and manifolds using the Bayesian Gaussian Mixture Model (GMM) [23]. In the case of graphs, the node update equation is defined as:

$$h_i^{\ell+1} = \text{ReLU}\left(\sum_{k=1}^K \sum_{j \in \mathcal{N}_i} e_{ij}^{k,\ell} U^{k,\ell} h_j^\ell\right), \quad (21)$$

$$e_{ij}^{k,\ell} = \exp\left(-\frac{1}{2}(u_{ij}^\ell - \mu_k^\ell)^T (\Sigma_k^\ell)^{-1} (u_{ij}^\ell - \mu_k^\ell)\right), \quad (22)$$

$$u_{ij}^\ell = \text{Tanh}\left(A^\ell (\text{deg}_i^{-1/2}, \text{deg}_j^{-1/2})^T + a^\ell\right), \quad (23)$$

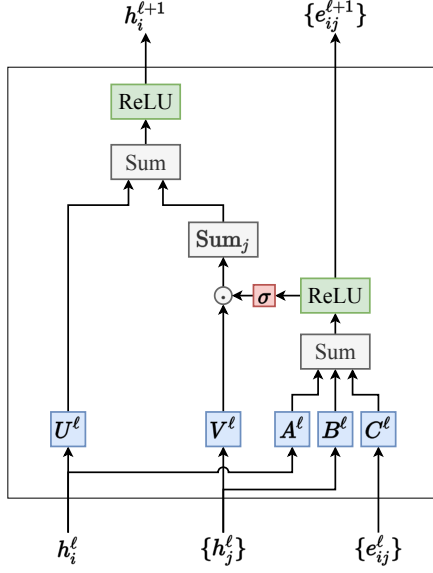


Figure 10: GatedGCN Layer

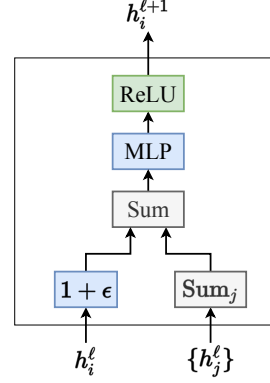


Figure 11: GIN Layer

where $U^{k,\ell} \in \mathbb{R}^{d \times d}$, $\mu_k^\ell, (\Sigma_k^\ell)^{-1}, a^\ell \in \mathbb{R}^2$ and $A^\ell \in \mathbb{R}^{2 \times 2}$ are the (learnable) parameters of the GMM, see Figure 9.

Gated Graph ConvNet (GatedGCN) [11] GatedGCN considers residual connections, batch normalization and edge gates to design another anisotropic variant of GCN. The authors propose to explicitly update edge features along with node features:

$$h_i^{\ell+1} = h_i^\ell + \text{ReLU}\left(\text{BN}\left(U^\ell h_i^\ell + \sum_{j \in \mathcal{N}_i} e_{ij}^\ell \odot V^\ell h_j^\ell\right)\right), \quad (24)$$

where $U^\ell, V^\ell \in \mathbb{R}^{d \times d}$, \odot is the Hadamard product, and the edge gates e_{ij}^ℓ are defined as:

$$e_{ij}^\ell = \frac{\sigma(\hat{e}_{ij}^\ell)}{\sum_{j' \in \mathcal{N}_i} \sigma(\hat{e}_{ij'}^\ell) + \varepsilon}, \quad (25)$$

$$\hat{e}_{ij}^\ell = \hat{e}_{ij}^{\ell-1} + \text{ReLU}\left(\text{BN}\left(A^\ell h_i^{\ell-1} + B^\ell h_j^{\ell-1} + C^\ell \hat{e}_{ij}^{\ell-1}\right)\right), \quad (26)$$

where σ is the sigmoid function, ε is a small fixed constant for numerical stability, $A^\ell, B^\ell, C^\ell \in \mathbb{R}^{d \times d}$, see Figure 10. Note that the edge gates (25) can be regarded as a soft attention process, related to the standard sparse attention mechanism [6]. Different from other anisotropic GNNs, the GatedGCN architecture explicitly maintains edge features \hat{e}_{ij} at each layer, following [12, 40].

Graph Isomorphism Networks (GIN) [89] The GIN architecture is based the Weisfeiler-Lehman Isomorphism Test [88] to study the expressive power of GNNs. The node update equation is defined as:

$$h_i^{\ell+1} = \text{ReLU}\left(U^\ell\left(\text{ReLU}\left(\text{BN}\left(V^\ell \hat{h}_i^{\ell+1}\right)\right)\right)\right), \quad (27)$$

$$\hat{h}_i^{\ell+1} = (1 + \epsilon) h_i^\ell + \sum_{j \in \mathcal{N}_i} h_j^\ell, \quad (28)$$

where ϵ is a learnable constant, $U^\ell, V^\ell \in \mathbb{R}^{d \times d}$, BN denotes Batch Normalization. See Figure 11 for illustration of the update equation.

Normalization and Residual Connections As a final note, we augment each message-passing GCN layer with batch normalization (BN) [36] and residual connections [34]. As such, we consider

a more specific class of GCNs than (11):

$$h_i^{\ell+1} = h_i^\ell + \sigma\left(\text{BN}\left(\hat{h}_i^{\ell+1}\right)\right), \quad (29)$$

$$\hat{h}_i^{\ell+1} = g_{\text{GCN}}\left(h_i^\ell, \{h_j^\ell : j \rightarrow i\}\right), \quad (30)$$

where σ is a non-linear activation function and g_{GCN} is a specific message-passing GCN layer.

B.1.3 Task-based Layer

The final component of each network is a prediction layer to compute task-dependent outputs, which are given to a loss function to train the network parameters in an end-to-end manner. The input of the prediction layer is the result of the final message-passing GCN layer for each node of the graph (except GIN, which uses features from all intermediate layers).

Graph classifier layer To perform graph classification, we first build a d -dimensional graph-level vector representation $y_{\mathcal{G}}$ by averaging over all node features in the final GCN layer:

$$y_{\mathcal{G}} = \frac{1}{V} \sum_{i=0}^V h_i^L, \quad (31)$$

The graph features are then passed to a MLP, which outputs un-normalized logits/scores $y_{\text{pred}} \in \mathbb{R}^C$ for each class:

$$y_{\text{pred}} = P \text{ReLU}(Q y_{\mathcal{G}}), \quad (32)$$

where $P \in \mathbb{R}^{d \times C}$, $Q \in \mathbb{R}^{d \times d}$, C is the number of classes. Finally, we minimize the cross-entropy loss between the logits and groundtruth labels.

Graph regression layer For graph regression, we compute $y_{\mathcal{G}}$ using Eq.(31) and pass it to a MLP which gives the prediction score $y_{\text{pred}} \in \mathbb{R}$:

$$y_{\text{pred}} = P \text{ReLU}(Q y_{\mathcal{G}}), \quad (33)$$

where $P \in \mathbb{R}^{d \times 1}$, $Q \in \mathbb{R}^{d \times d}$. The L1-loss between the predicted score and the groundtruth score is minimized during the training.

Node classifier layer For node classification, we independently pass each node's feature vector to a MLP for computing the un-normalized logits $y_{i,\text{pred}} \in \mathbb{R}^C$ for each class:

$$y_{i,\text{pred}} = P \text{ReLU}(Q h_i^L), \quad (34)$$

where $P \in \mathbb{R}^{d \times C}$, $Q \in \mathbb{R}^{d \times d}$. The cross-entropy loss weighted inversely by the class size is used during training.

Edge classifier layer To make a prediction for each graph edge e_{ij} , we first concatenate node features h_i and h_j from the final GNN layer. The concatenated edge features are then passed to a MLP for computing the un-normalized logits $y_{ij,\text{pred}} \in \mathbb{R}^C$ for each class:

$$y_{ij,\text{pred}} = P \text{ReLU}(Q \text{Concat}(h_i^L, h_j^L)), \quad (35)$$

where $P \in \mathbb{R}^{d \times C}$, $Q \in \mathbb{R}^{d \times 2d}$. The standard cross-entropy loss between the logits and groundtruth labels is used.

B.2 Weisfeiler-Lehman GNNs

B.2.1 Input Tensor

For a given graph with adjacency matrix $A \in \mathbb{R}^{n \times n}$, node features $h^{\text{node}} \in \mathbb{R}^{n \times d}$ and edge features $h^{\text{edge}} \in \mathbb{R}^{n \times n \times d_e}$, the input tensor to the RingGNN and 3WL-GNN networks is defined as

$$h^{\ell=0} \in \mathbb{R}^{n \times n \times (1+d+d_e)}, \quad (36)$$

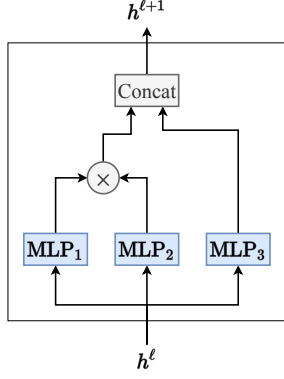


Figure 12: 3WL-GNN Layer

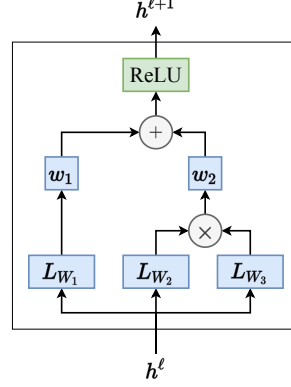


Figure 13: RingGNN Layer

where

$$h_{i,j,1}^{\ell=0} = A_{ij} \in \mathbb{R}, \quad \forall i, j \quad (37)$$

$$h_{i,j,2:d+1}^{\ell=0} = \begin{cases} h_i^{\text{node}} \in \mathbb{R}^d, & \forall i = j \\ 0, & \forall i \neq j \end{cases} \quad (38)$$

$$h_{i,j,d+2:d+d_e+1}^{\ell=0} = h_{ij}^{\text{edge}} \in \mathbb{R}^{d_e} \quad (39)$$

B.2.2 WL-GNN layers

3WL-GNNs [58] These networks introduced an architecture that can distinguish two non-isomorphic graphs with the 3-WL test. The layer update equation of 3WL-GNNs is defined as:

$$h^{\ell+1} = \text{Concat}\left(M_{W_1}^\ell(h^\ell) \cdot M_{W_2}^\ell(h^\ell), M_{W_3}^\ell(h^\ell)\right), \quad (40)$$

where $h^\ell, h^{\ell+1} \in \mathbb{R}^{n \times n \times d}$, and M_W are 2-layer MLPs applied along the feature dimension:

$$M_{W=\{W_a, W_b\}}(h) = \sigma(h W_a) W_b, \quad (41)$$

where $W_a, W_b \in \mathbb{R}^{d \times d}$. As $h \in \mathbb{R}^{n \times n \times d}$, the MLP (41) is implemented with a standard 2D-convolutional layer with 1×1 kernel size. Eventually, the matrix multiplication in (40) is carried out along the first and second dimensions such that:

$$\left(M_{W_1}(h) \cdot M_{W_2}(h)\right)_{i,j,k} = \sum_{p=1}^n \left(M_{W_1}(h)\right)_{i,p,k} \cdot \left(M_{W_2}(h)\right)_{p,j,k}, \quad (42)$$

with complexity $O(n^3)$.

Ring-GNNs [18] These models proposed to improve the order-2 equivariant GNNs of [59] with the multiplication of two equivariant linear layers. The layer update equation of Ring-GNNs is designed as:

$$h^{\ell+1} = \sigma\left(w_1^\ell L_{W_1}^\ell(h^\ell) + w_2^\ell L_{W_2}^\ell(h^\ell) \cdot L_{W_3}^\ell(h^\ell)\right), \quad (43)$$

where $h^\ell, h^{\ell+1} \in \mathbb{R}^{n \times n \times d}$, $w_{1,2}^\ell \in \mathbb{R}$, and L_W are the equivariant linear layers defined as

$$\left(L_W(h)\right)_{i,j,k} = \sum_{p=1}^{17} \sum_{q=1}^d W_{p,q,k} \left(L_i(h)\right)_{i,j,q}, \quad (44)$$

where $W \in \mathbb{R}^{d \times d \times 17}$ and $\{L_i\}_{i=1}^{15}$ is the set of all basis functions for all linear equivariant functions from $\mathbb{R}^{n \times n} \rightarrow \mathbb{R}^{n \times n}$ (see Appendix A in [59] for the complete list of these 15 operations) and $\{L_i\}_{i=16}^{17}$ are the basis for the bias terms. Matrix multiplication in (43) also implies a time complexity $O(n^3)$.

B.2.3 Task-based network layers

We describe the final network layers depending on the task at hand. The loss functions corresponding to the task are the same as the GCNs, and presented in Section B.1.3.

Graph classifier layer We have followed the original author implementations in [58, 59, 18] to design the classifier layer for 3WL-GNNs and Ring-GNNs. Similar to [90, 89], the classifier layer for Ring-GNNs uses features from all intermediate layers and then passes the features to a MLP:

$$y_G = \text{Concat}_{\ell=1}^L \left(\sum_{i,j=1}^n h_{ij}^\ell \right) \in \mathbb{R}^{Ld}, \quad (45)$$

$$y_{\text{pred}} = P \text{ReLU} (Q y_G) \in \mathbb{R}^C, \quad (46)$$

where $P \in \mathbb{R}^{d \times C}$, $Q \in \mathbb{R}^{Ld \times d}$, C is the number of classes.

For 3WL-GNNs, Eqn. (45) is replaced by a diagonal and off-diagonal max pooling readout [58, 59] at every layer:

$$y_G^\ell = \text{Concat} \left(\max_i h_{ii}^\ell, \max_{i \neq j} h_{ij}^\ell \right) \in \mathbb{R}^{2d}, \quad (47)$$

and the final prediction score is defined as:

$$y_{\text{pred}} = \sum_{\ell=1}^L P^\ell y_G^\ell \in \mathbb{R}^C, \quad (48)$$

where $P^\ell \in \mathbb{R}^{2d \times C}$, C is the number of classes.

Graph regression layer Similar to the graph classifier layer with $P \in \mathbb{R}^{d \times 1}$ for Ring-GNNs, and $P^\ell \in \mathbb{R}^{2d \times 1}$ for 3WL-GNNs.

Node classifier layer For node classification, the prediction in Ring-GNNs is done as follows:

$$y_i^{\text{node}} = \text{Concat}_{\ell=1}^L \left(\sum_{j=1}^n h_{ij}^\ell \right) \in \mathbb{R}^{Ld}, \quad (49)$$

$$y_{i,\text{pred}} = P \text{ReLU} (Q y_i^{\text{node}}) \in \mathbb{R}^C, \quad (50)$$

where $P \in \mathbb{R}^{d \times C}$, $Q \in \mathbb{R}^{Ld \times d}$, C is the number of classes.

In 3WL-GNNs, the final prediction score is defined as:

$$y_i^{\text{node},\ell} = \sum_{j=1}^n h_{ij}^\ell \in \mathbb{R}^d, \quad (51)$$

$$y_{i,\text{pred}} = \sum_{\ell=1}^L P^\ell y_i^{\text{node},\ell} \in \mathbb{R}^C, \quad (52)$$

where $P^\ell \in \mathbb{R}^{d \times C}$, C is the number of classes.

Edge classifier layer For link prediction, for both Ring-GNNs and 3WL-GNNs, the edge features are obtained by concatenating the node features such as:

$$y_i^{\text{node}} = \text{Concat}_{\ell=1}^L \left(\sum_{j=1}^n h_{ij}^\ell \right) \in \mathbb{R}^{Ld}, \quad (53)$$

$$y_{ij,\text{pred}} = P \text{ReLU} (Q \text{Concat} (y_i^{\text{node}}, y_j^{\text{node}})) \in \mathbb{R}^C, \quad (54)$$

where $P \in \mathbb{R}^{d \times C}$, $Q \in \mathbb{R}^{2Ld \times d}$, C is the number of classes.

Table 6: Performance on the TU datasets with 10-fold cross validation (higher is better). Two runs of all the experiments using the same hyperparameters but different random seeds are shown separately to note the differences in ranking and variation for reproducibility. The top 3 performance scores are highlighted as **First**, **Second**, **Third**.

Dataset	Model	L	#Param	seed 1				seed 2			
				Test Acc. \pm s.d.	Train Acc. \pm s.d.	#Epoch	Epoch/Total	Test Acc. \pm s.d.	Train Acc. \pm s.d.	#Epoch	Epoch/Total
ENZYMES	MLP	4	101481	55.833 \pm 3.516	93.062 \pm 7.551	332.30	0.18s/0.17hr	53.833 \pm 4.717	87.854 \pm 10.765	327.80	0.19s/0.18hr
	GCN	4	103407	65.833\pm4.610	97.688 \pm 3.064	343.00	0.69s/0.67hr	64.833 \pm 7.089	93.042 \pm 4.982	334.30	0.74s/0.70hr
	GraphSage	4	105595	65.000 \pm 4.944	100.000 \pm 0.000	294.20	1.62s/1.34hr	68.167\pm5.449	100.000 \pm 0.000	287.30	1.76s/1.42hr
	MoNet	4	105307	63.000 \pm 8.090	95.229 \pm 5.864	333.70	0.53s/0.49hr	62.167 \pm 4.833	93.562 \pm 5.897	324.40	0.68s/0.62hr
	GAT	4	101274	68.500\pm5.241	100.000 \pm 0.000	299.30	0.70s/0.59hr	68.500\pm4.622	100.000 \pm 0.000	309.10	0.76s/0.66hr
	GatedGCN	4	103409	65.667\pm4.899	99.979 \pm 0.062	316.80	2.31s/2.05hr	70.000\pm4.944	99.979 \pm 0.062	313.20	2.63s/2.30hr
	GIN	4	104864	65.333 \pm 6.823	100.000 \pm 0.000	402.10	0.53s/0.61hr	67.667 \pm 5.831	100.000 \pm 0.000	404.90	0.60s/0.68hr
	RingGNN	2	103538	18.667 \pm 1.795	20.104 \pm 2.166	337.30	7.12s/6.71hr	45.333 \pm 4.522	56.792 \pm 6.081	497.50	8.05s/11.16hr
	3WLGNN	3	104658	61.000 \pm 6.799	98.875 \pm 1.571	381.80	9.22s/9.83hr	57.667 \pm 9.522	96.729 \pm 5.525	336.50	11.80s/11.09hr
	MLP	4	100447	72.239 \pm 3.854	73.816 \pm 1.015	371.80	6.36s/6.61hr	72.408\pm3.449	73.880 \pm 0.623	349.60	1.13s/1.11hr
DD	GCN	4	102293	72.758 \pm 4.083	100.000 \pm 0.000	266.70	3.56s/2.66hr	73.168\pm5.000	100.000 \pm 0.000	270.20	3.81s/2.88hr
	GraphSage	4	102577	73.433\pm3.429	100.000 \pm 0.000	267.20	11.50s/8.59hr	71.900 \pm 3.647	100.000 \pm 0.000	265.50	6.60s/4.90hr
	MoNet	4	102305	71.736 \pm 3.365	81.003 \pm 2.593	252.60	3.30s/2.34hr	71.479 \pm 2.167	81.268 \pm 2.295	253.50	2.83s/2.01hr
	GAT	4	100132	75.900\pm3.824	95.851 \pm 2.575	201.30	6.31s/3.56hr	74.198\pm3.076	96.964 \pm 1.544	220.10	2.84s/1.75hr
	GatedGCN	4	104165	72.918\pm2.090	82.796 \pm 2.242	300.70	12.05s/10.13hr	71.983 \pm 3.644	83.243 \pm 3.716	323.60	8.78s/7.93hr
	GIN	4	103046	71.910 \pm 3.873	99.851 \pm 0.136	275.70	5.28s/4.08hr	70.883 \pm 2.702	99.883 \pm 0.088	276.90	2.31s/1.79hr
	RingGNN	2	109857	OOM	OOM	OOM	OOM	OOM	OOM	OOM	OOM
	3WLGNN	3	104124	OOM	OOM	OOM	OOM	OOM	OOM	OOM	OOM
	MLP	4	100643	75.644 \pm 2.681	79.847 \pm 1.551	244.20	0.42s/0.29hr	75.823 \pm 2.915	79.442 \pm 1.443	241.20	0.35s/0.24hr
	GCN	4	104865	76.098 \pm 2.406	81.387 \pm 2.451	350.90	1.55s/1.53hr	75.912\pm3.064	82.140 \pm 2.706	349.60	1.46s/1.42hr
PROTEINS	GraphSage	4	101928	75.289 \pm 2.419	85.827 \pm 0.839	245.40	3.36s/2.30hr	75.559 \pm 1.907	85.118 \pm 1.171	244.40	3.44s/2.35hr
	MoNet	4	103858	76.452\pm2.898	78.206 \pm 0.548	306.80	1.23s/1.06hr	76.453\pm2.892	78.273 \pm 0.695	289.50	1.26s/1.03hr
	GAT	4	102710	76.277\pm2.410	83.186 \pm 2.000	344.60	1.47s/1.42hr	75.557 \pm 3.443	84.253 \pm 2.348	335.10	1.51s/1.41hr
	GatedGCN	4	104855	76.363\pm2.904	79.431 \pm 0.695	293.80	5.03s/4.13hr	76.721\pm3.106	78.689 \pm 0.692	272.80	4.78s/3.64hr
	GIN	4	103854	74.117 \pm 3.357	75.351 \pm 1.267	420.90	1.02s/1.20hr	71.241 \pm 4.921	71.373 \pm 2.835	362.00	1.04s/1.06hr
	RingGNN	2	109036	67.564 \pm 7.551	67.607 \pm 4.401	150.40	28.61s/12.08hr	56.063 \pm 6.301	59.289 \pm 5.560	222.70	19.08s/11.88hr
	3WLGNN	3	105366	61.712 \pm 4.859	62.427 \pm 4.548	211.40	12.82s/7.58hr	64.682 \pm 5.877	65.034 \pm 5.253	200.40	13.05s/7.32hr

C Experiments on TU datasets

Apart from the proposed datasets in our benchmark (Section 3), we perform experiments on 3 TU datasets for graph classification – ENZYMES, DD and PROTEINS. Our goal is to empirically highlight some of the challenges of using these conventional datasets for benchmarking GNNs.

Splitting. Since the 3 TU datasets that we use do not have standard splits, we perform a 10-fold cross validation split which gives 10 sets of train, validation and test data indices in the ratio 8 : 1 : 1. We use stratified sampling to ensure that the class distribution remains the same across splits. The indices are saved and used across all experiments for fair comparisons. There are 480 train/60 validation/60 test graphs for ENZYMES, 941 train/118 validation/119 test graphs for DD, and 889 train/112 validation/112 test graphs for PROTEINS datasets in each of the folds.

Training. We use Adam optimizer with a similar learning rate strategy as used in our benchmark’s experimental protocol. An initial learning rate is tuned from a range of 1×10^{-3} to 7×10^{-5} using grid search for every GNN models. The learning rate reduce factor is 0.5, the patience value is 25 and the stopping learning rate is 1×10^{-6} .

Performance Measure. We use classification accuracy between the predicted labels and groundtruth labels as our performance measure. The model performance is evaluated on the test split of the 10 folds for all TU datasets, and reported as the average and the standard deviation of the 10 scores.

Our numerical results on the TU datasets – ENZYMES, DD and PROTEINS are presented in Table 6. We observe all NNs have similar statistical test performance as the standard deviation is quite large. We also report a second run of these experiments with the same experimental protocol, *i.e.* the same 10-fold splitting and hyperparameters but different initialization (seed). We observe a change of model ranking, which we attribute to the small size of the datasets and the non-determinism of gradient descent optimizers. We also observe that, for DD and PROTEINS, the graph-agnostic MLP baselines perform as good as GNNs. Our observations reiterate how experiments on the small TU datasets are difficult to determine which GNNs are powerful and robust.

D Laplacian Positional Encodings

Standard GCNs are not able to differentiate isomorphic nodes [67, 93]. To overcome this issue, positional encoding (PE) of nodes was proposed. Ideally, PEs should be unique for each node, and nodes which are far apart in the graph should have different positional features whereas nodes which are nearby have similar positional features. Note that in a graph that has some symmetries, positional features cannot be assigned in a canonical way. For example, if node i and node j are

structurally symmetric, and we have positional features $p_i = a, p_j = b$ that differentiate them, then it is also possible to arbitrary choose $p_i = b, p_j = a$ since i and j are completely symmetric by definition. In other words, the PE is always arbitrary up to the number of symmetries in the graph. As a consequence, the network will have to learn to deal with these ambiguities during training. The simplest possible positional encodings is to give an (arbitrary) ordering to the nodes, among $n!$ possible orderings. During training, the orderings are uniformly sampled from the $n!$ possible choices in order for the network to learn to be independent to these arbitrary choices [67].

We propose an alternative to reduce the sampling space, and therefore the amount of ambiguities to be resolved by the network. Laplacian eigenvectors are hybrid positional and structural encodings, as they are invariant by node re-parametrization. However, they are also limited by natural symmetries such as the arbitrary sign of eigenvectors (after being normalized to have unit length). The number of possible sign flips is 2^k , where k is the number of eigenvectors. In practice we choose $k \ll n$, and therefore 2^k is much smaller $n!$ (the number of possible ordering of the nodes). During the training, the eigenvectors will be uniformly sampled at random between the 2^k possibilities. If we do not seek to learn the invariance w.r.t. all possible sign flips of eigenvectors, then we can remove the sign ambiguity of eigenvectors by taking the absolute value. This choice seriously degrades the expressivity power of the positional features.

Numerical results for different positional encodings are reported in Table 7. For all results, we use the GatedGCN model [11]. We study 5 types of positional encodings; *EigVecs-k* corresponds to the smallest non-trivial k eigenvectors, *Rand sign(EigVecs)* randomly flips the sign of the k smallest non-trivial eigenvectors in each batch, *Abs(EigVecs)* takes the absolute value of the k eigenvectors, *Fixed node ordering* uses the original node ordering of graphs, and *Rand node ordering* randomly permutes ordering of nodes in each batch. We observed that the best results are consistently produced with the Laplacian PEs with random sign flipping at training. For index PEs, randomly permuting the ordering of nodes also improves significantly the performances over keeping fixed the original node ordering. However, Laplacian PEs clearly outperform index PEs.

Table 7: Study of positional encodings (PEs) with the GatedGCN model [11]. Performance reported on the test sets of CSL, ZINC, PATTERN, CLUSTER and COLLAB (higher is better, except for ZINC). **Red**: the best model.

	PE type	L	#Param	Test Acc. \pm s.d.	Train Acc. \pm s.d.	#Epochs	Epoch/Total
CSL	No PE	4	104007	10.000 \pm 0.000	10.000 \pm 0.000	54.00	0.58s/0.05hr
	EigVecs-20	4	105407	68.633 \pm 7.143	99.811 \pm 0.232	107.16	0.59s/0.09hr
	Rand sign(EigVecs)	4	105407	99.767\pm0.394	99.689 \pm 0.550	188.76	0.59s/0.16hr
	Abs(EigVecs)	4	105407	99.433 \pm 1.133	100.000 \pm 0.000	143.64	0.60s/0.12hr
	Fixed node ordering	4	106807	10.533 \pm 4.469	76.056 \pm 14.136	60.56	0.59s/0.05hr
	Rand node ordering	4	106807	11.133 \pm 2.571	10.944 \pm 2.106	91.60	0.60s/0.08hr
PATTERN	No PE	16	502223	85.605 \pm 0.105	85.999 \pm 0.145	62.00	646.03s/11.36hr
	EigVecs-2	16	505421	86.029 \pm 0.085	86.955 \pm 0.227	65.00	645.36s/11.94hr
	Rand sign(EigVecs)	16	502457	86.508\pm0.085	86.801 \pm 0.133	65.75	647.94s/12.08hr
	Abs(EigVecs)	16	505421	86.393 \pm 0.037	87.011 \pm 0.172	62.00	645.90s/11.41hr
	Fixed node ordering	16	516887	80.133 \pm 0.202	98.416 \pm 0.141	45.00	643.23s/8.27hr
	Rand node ordering	16	516887	85.767 \pm 0.044	85.998 \pm 0.063	64.50	645.09s/11.79hr
CLUSTER	No PE	16	502615	73.684 \pm 0.348	88.356 \pm 1.577	61.50	399.44s/6.97hr
	EigVecs-20	16	504253	75.520 \pm 0.395	89.332 \pm 1.297	49.75	400.50s/5.70hr
	Rand sign(EigVecs)	16	504253	76.082\pm0.196	88.919 \pm 0.720	57.75	399.66s/6.58hr
	Abs(EigVecs)	16	504253	73.796 \pm 0.234	91.125 \pm 1.248	58.75	398.97s/6.68hr
	Fixed node ordering	16	517435	69.232 \pm 0.265	92.298 \pm 0.712	51.00	400.40s/5.82hr
	Rand node ordering	16	517435	74.656 \pm 0.314	82.940 \pm 1.718	61.00	397.75s/6.88hr
COLLAB	No PE	3	40965	52.635 \pm 1.168	96.103 \pm 1.876	95.00	453.47s/12.09hr
	EigVecs-20	3	41889	52.326 \pm 0.678	96.700 \pm 1.296	95.00	452.40s/12.10hr
	Rand sign(EigVecs)	3	41889	52.849\pm1.345	96.165 \pm 0.453	94.75	452.75s/12.08hr
	Abs(EigVecs)	3	41889	51.419 \pm 1.109	95.984 \pm 1.157	95.00	451.36s/12.07hr
	PE type	L	#Param	Test MAE \pm s.d.	Train MAE \pm s.d.	#Epochs	Epoch/Total
ZINC	No PE	16	504153	0.354 \pm 0.012	0.095 \pm 0.012	165.25	10.52s/0.49hr
	EigVecs-8	16	505011	0.319 \pm 0.010	0.038 \pm 0.007	143.25	10.62s/0.43hr
	Rand sign(EigVecs)	16	505011	0.214\pm0.013	0.067 \pm 0.019	185.00	10.70s/0.56hr
	Abs(EigVecs)	16	505011	0.214\pm0.009	0.035 \pm 0.011	167.50	10.61s/0.50hr
	Fixed node ordering	16	507195	0.431 \pm 0.007	0.044 \pm 0.009	118.25	10.62s/0.35hr
	Rand node ordering	16	507195	0.321 \pm 0.015	0.177 \pm 0.015	184.75	10.55s/0.55hr

E Dissecting GNNs for Edge Representation Analysis

In Section 4, Table 4, we systematically study the impact of anisotropy by instantiating three variants of GAT and GatedGCN: (1) Isotropic aggregation, such as vanilla GCNs, Eq.(13); (2) Anisotropy using edge features, such as GAT by default, Eq.(18); and (3) Anisotropy with edge features and explicit edge representations updated at each layer, such as in GatedGCN by default, Eq.(24). This section provides formal equations for each model variant. (Note that there may be a multitude of approaches to instantiating anisotropic GNNs and using edge features [8, 74, 13] besides the ones we consider.)

E.1 GatedGCN

Isotropic, similar to vanilla GCNs with sum aggregation:

$$h_i^{\ell+1} = h_i^\ell + \text{ReLU}\left(\text{BN}\left(U^\ell h_i^\ell + \sum_{j \in \mathcal{N}_i} V^\ell h_j^\ell\right)\right), \quad \text{where } U^\ell, V^\ell \in \mathbb{R}^{d \times d}. \quad (55)$$

Anisotropic with intermediate edge features computed as joint representations of adjacent node features at each layer:

$$h_i^{\ell+1} = h_i^\ell + \text{ReLU}\left(\text{BN}\left(U^\ell h_i^\ell + \sum_{j \in \mathcal{N}_i} e_{ij}^\ell \odot V^\ell h_j^\ell\right)\right), \quad (56)$$

$$e_{ij}^\ell = \frac{\sigma(\hat{e}_{ij}^\ell)}{\sum_{j' \in \mathcal{N}_i} \sigma(\hat{e}_{ij'}^\ell) + \varepsilon}, \quad \hat{e}_{ij}^\ell = A^\ell h_i^{\ell-1} + B^\ell h_j^{\ell-1}, \quad (57)$$

where $U^\ell, V^\ell \in \mathbb{R}^{d \times d}$, \odot is the Hadamard product, and e_{ij}^ℓ are the edge gates.

Anisotropic with edge features as well as explicit edge representations updated across layers in addition to node features, as in GatedGCN by default, Eq.(24):

$$h_i^{\ell+1} = h_i^\ell + \text{ReLU}\left(\text{BN}\left(U^\ell h_i^\ell + \sum_{j \in \mathcal{N}_i} e_{ij}^\ell \odot V^\ell h_j^\ell\right)\right), \quad (58)$$

$$e_{ij}^\ell = \frac{\sigma(\hat{e}_{ij}^\ell)}{\sum_{j' \in \mathcal{N}_i} \sigma(\hat{e}_{ij'}^\ell) + \varepsilon}, \quad (59)$$

$$\hat{e}_{ij}^\ell = \hat{e}_{ij}^{\ell-1} + \text{ReLU}\left(\text{BN}\left(A^\ell h_i^{\ell-1} + B^\ell h_j^{\ell-1} + C^\ell \hat{e}_{ij}^{\ell-1}\right)\right), \quad (60)$$

where $U^\ell, V^\ell \in \mathbb{R}^{d \times d}$, \odot is the Hadamard product, and e_{ij}^ℓ are the edge gates. The input edge features from the datasets (e.g. distances for TSP, collaboration year and frequency for COLLAB) can optionally be used to initialize the edge representations $\hat{e}_{ij}^{\ell=0}$.

E.2 GAT

Isotropic, similar to multi-headed vanilla GCNs with sum aggregation:

$$h_i^{\ell+1} = \text{Concat}_{k=1}^K \left(\text{ELU}\left(\text{BN}\left(\sum_{j \in \mathcal{N}_i} U^{k,\ell} h_j^\ell\right)\right) \right), \quad \text{where } U^{k,\ell} \in \mathbb{R}^{\frac{d}{K} \times d}. \quad (61)$$

Anisotropic with intermediate edge features computed as joint representations of adjacent node features at each layer, as in GAT by default, Eq.(18):

$$h_i^{\ell+1} = h_i^\ell + \text{ELU}\left(\text{BN}\left(\text{Concat}_{k=1}^K \left(\sum_{j \in \mathcal{N}_i} e_{ij}^{k,\ell} U^{k,\ell} h_j^\ell \right) \right) \right), \quad (62)$$

$$e_{ij}^{k,\ell} = \frac{\exp(\hat{e}_{ij}^{k,\ell})}{\sum_{j' \in \mathcal{N}_i} \exp(\hat{e}_{ij'}^{k,\ell})}, \quad \hat{e}_{ij}^{k,\ell} = \text{LeakyReLU}\left(V^{k,\ell} \text{Concat}(U^{k,\ell} h_i^\ell, U^{k,\ell} h_j^\ell)\right), \quad (63)$$

where $U^{k,\ell} \in \mathbb{R}^{\frac{d}{K} \times d}$, $V^{k,\ell} \in \mathbb{R}^{\frac{2d}{K} \times d}$ are the K linear projection heads and $e_{ij}^{k,\ell}$ are the attention coefficients for each head.

Table 8: Study of anisotropic edge features and representations for link prediction on COLLAB, including GraphSage models. **Red**: the best model, **Violet**: good models.

Model	Edge Feat.	Edge Repr.	Aggregation Function	L	#Param	Test Acc. \pm s.d.	Train Acc. \pm s.d.	#Epoch	Epoch/Total
GatedGCN	\times	\times	Sum	3	26593	35.989 \pm 1.549	60.586 \pm 4.251	148.00	263.62s/10.90h
	\checkmark	\times	Weighted Mean	3	26715	50.668\pm0.291	96.128 \pm 0.576	172.00	384.39s/18.44hr
	\checkmark	\checkmark	Weighted Mean	3	27055	51.537\pm1.038	96.524 \pm 1.704	188.67	376.67s/19.85hr
GatedGCN-E	\checkmark	\checkmark	Weighted Mean	3	27055	47.212 \pm 2.016	85.801 \pm 0.984	156.67	377.04s/16.49hr
GAT	\times	\times	Sum	3	28201	41.141 \pm 0.701	70.344 \pm 1.837	153.50	371.50s/15.97hr
	\checkmark	\times	Weighted Mean	3	28561	50.662\pm0.687	96.085 \pm 0.499	174.50	403.52s/19.69hr
	\checkmark	\checkmark	Weighted Mean	3	26676	49.674\pm0.105	92.665 \pm 0.719	201.00	349.19s/19.59hr
GAT-E	\checkmark	\checkmark	Weighted Mean	3	26676	44.989 \pm 1.395	82.230 \pm 4.941	120.67	328.29s/11.10hr
GraphSage	\times	\times	Max	3	26293	50.908\pm1.122	98.617 \pm 1.763	157.75	241.49s/10.62hr
	\checkmark	\times	Weighted Max	3	26487	50.997\pm0.875	99.158 \pm 0.694	112.00	366.24s/11.46hr
	\checkmark	\checkmark	Weighted Max	3	26950	48.530 \pm 1.919	90.990 \pm 9.273	118.25	359.18s/11.88hr
GraphSage-E	\checkmark	\checkmark	Weighted Max	3	26950	47.315 \pm 1.939	93.475 \pm 5.884	120.00	359.10s/12.07hr

Anisotropic with edge features as well as explicit edge representations updated across layers in addition to node features:

$$h_i^{\ell+1} = h_i^\ell + \text{ELU}\left(\text{BN}\left(\text{Concat}_{k=1}^K\left(\sum_{j \in \mathcal{N}_i} a_{ij}^{k,\ell} U^{k,\ell} h_j^\ell\right)\right)\right), \quad (64)$$

$$e_{ij}^{\ell+1} = e_{ij}^\ell + \text{ELU}\left(\text{BN}\left(\text{Concat}_{k=1}^K\left(B^{k,\ell} \text{Concat}\left(A^{k,\ell} e_{ij}^\ell, U^{k,\ell} h_i^\ell, U^{k,\ell} h_j^\ell\right)\right)\right)\right), \quad (65)$$

$$a_{ij}^{k,\ell} = \frac{\exp(\hat{a}_{ij}^{k,\ell})}{\sum_{j' \in \mathcal{N}_i} \exp(\hat{a}_{ij'}^{k,\ell})}, \quad (66)$$

$$\hat{a}_{ij}^{k,\ell} = \text{LeakyReLU}\left(V^{k,\ell} \text{Concat}\left(A^{k,\ell} e_{ij}^\ell, U^{k,\ell} h_i^\ell, U^{k,\ell} h_j^\ell\right)\right), \quad (67)$$

where $U^{k,\ell} \in \mathbb{R}^{\frac{d}{K} \times d}$, $V^{k,\ell} \in \mathbb{R}^{\frac{3d}{K}}$, $A^{k,\ell} \in \mathbb{R}^{\frac{d}{K} \times d}$, $B^{k,\ell} \in \mathbb{R}^{\frac{d}{K} \times \frac{3d}{K}}$ are the K linear projection heads and $a_{ij}^{k,\ell}$ are the attention coefficients for each head. The input edge features from the datasets can optionally be used to initialize the edge representations $e_{ij}^{\ell=0}$.

E.3 GraphSage

Interestingly, in Table 2 for COLLAB, we found that the isotropic GraphSage with max aggregation performs close to GAT and GatedGCN models, both of which perform anisotropic mean aggregation. On the other hand, models which use sum aggregation (GIN, MoNet) are unable to beat the simple matrix factorization baseline. This result indicates that aggregation functions which are invariant to node degree (max and mean) provide a powerful inductive bias for COLLAB.

We instantiate two anisotropic variants of GraphSage, as described in the following paragraphs, and compare them to GAT and GatedGCN on COLLAB in Table 8. We find that upgrading max aggregators with edge features does not significantly boost performance. On the other hand, maintaining explicit edge representations across layers hurts the models, presumably due to using very small hidden dimensions. (As previously mentioned, maintaining representations for both 235K nodes and 2.3M edges leads to significant GPU memory usage and requires using smaller hidden dimensions.)

Isotropic, as in GraphSage by default, Eq.(16):

$$h_i^{\ell+1} = h_i^\ell + \text{ReLU}\left(\text{BN}\left(U^\ell \text{Concat}\left(h_i^\ell, \text{Max}_{j \in \mathcal{N}_i} \text{ReLU}\left(V^\ell h_j^\ell\right)\right)\right)\right), \quad (68)$$

where $U^\ell \in \mathbb{R}^{d \times 2d}$, $V^\ell \in \mathbb{R}^{d \times d}$.

Anisotropic with intermediate edge features computed as joint representations of adjacent node features at each layer:

$$h_i^{\ell+1} = h_i^\ell + \text{ReLU}\left(\text{BN}\left(U^\ell \text{Concat}\left(h_i^\ell, \text{Max}_{j \in \mathcal{N}_i} \text{ReLU}\left(\sigma\left(e_{ij}^\ell\right) \odot V^\ell h_j^\ell\right)\right)\right)\right), \quad (69)$$

$$e_{ij}^\ell = A^\ell\left(h_i^{\ell-1} + h_j^{\ell-1}\right), \quad (70)$$

where $U^\ell \in \mathbb{R}^{d \times 2d}$, $V^\ell, A^\ell \in \mathbb{R}^{d \times d}$, \odot is the Hadamard product, and e_{ij}^ℓ are the edge gates.

Anisotropic with edge features as well as explicit edge representations updated across layers in addition to node features:

$$h_i^{\ell+1} = h_i^\ell + \text{ReLU}\left(\text{BN}\left(U^\ell \text{Concat}\left(h_i^\ell, \text{Max}_{j \in \mathcal{N}_i} \text{ReLU}\left(\sigma\left(\hat{e}_{ij}^\ell \odot V^\ell h_j^\ell\right)\right)\right)\right)\right), \quad (71)$$

$$\hat{e}_{ij}^\ell = A^\ell (h_i^{\ell-1} + h_j^{\ell-1}) + B^\ell e_{ij}^{\ell-1}, \quad e_{ij}^{\ell+1} = e_{ij}^\ell + \text{ReLU}\left(\text{BN}\left(\hat{e}_{ij}^\ell\right)\right), \quad (72)$$

where $U^\ell \in \mathbb{R}^{d \times 2d}$, $V^\ell, A^\ell, B^\ell \in \mathbb{R}^{d \times d}$, \odot is the Hadamard product, and \hat{e}_{ij}^ℓ are the edge gates. The input edge features from the datasets can optionally be used to initialize the edge representations $e_{ij}^{\ell=0}$.

F A Note on Graph Size Normalization

Intuitively, batching graphs of variable sizes may lead to node representation at different scales, making it difficult to learn the optimal statistics μ and σ for BatchNorm across irregular batch sizes and variable graphs. A preliminary version of this work introduced a graph size normalization technique called GraphNorm, which normalizes the node features h_i^ℓ w.r.t. the graph size, *i.e.*,

$$\bar{h}_i^\ell = h_i^\ell \times \frac{1}{\sqrt{\mathcal{V}}}, \quad (73)$$

where \mathcal{V} is the number of graph nodes. The GraphNorm layer is placed before the BatchNorm layer.

We would like to note that GraphNorm does not have any concrete theoretical basis as of now, and was proposed based on initially promising empirical results on datasets such as ZINC and CLUSTER. Future work shall investigate more principled approaches towards designing normalization layers for graph structured data.

G Hardware Details

Timing research code can be tricky due to differences of implementations and hardware acceleration. Nonetheless, we take a practical view and report the average wall clock time per epoch and the total training time for each model. All experiments were implemented in DGL/PyTorch. We run experiments for MNIST, CIFAR10, ZINC, TSP, COLLAB and TUs on an Intel Xeon CPU E5-2690 v4 server with 4 Nvidia 1080Ti GPUs, and for PATTERN and CLUSTER on an Intel Xeon Gold 6132 CPU with 4 Nvidia 2080Ti GPUs. Each experiment was run on a single GPU and 4 experiments were run on the server at any given time (on different GPUs). We run each experiment for a maximum of 12 hours.